JEM Journal of Experimental Medicine

ARTICLE

Exit from germinal center to become quiescent memory B cells depends on metabolic reprograming and provision of a survival signal

Takeshi Inoue[1], Ryo Shinnakasu[1], Chie Kawai[1], Wataru Ise[1], Eiryo Kawakami[2,3], Nicolas Sax[4], Toshihiko Oki[5], Toshio Kitamura[5], Kazuo Yamashita[4], Hidehiro Fukuyama[6], and Tomohiro Kurosaki[1,6]

A still unanswered question is what drives the small fraction of activated germinal center (GC) B cells to become long-lived quiescent memory B cells. We found here that a small population of GC-derived CD38^{int}Bcl6$^{hi/int}$Efnb1^{+} cells with lower mTORC1 activity favored the memory B cell fate. Constitutively high mTORC1 activity led to defects in formation of the CD38^{int}Bcl6$^{hi/int}$Efnb1^{+} cells; conversely, decreasing mTORC1 activity resulted in relative enrichment of this memory-prone population over the recycling-prone one. Furthermore, the CD38^{int}Bcl6$^{hi/int}$Efnb1^{+} cells had higher levels of Bcl2 and surface BCR that, in turn, contributed to their survival and development. We also found that downregulation of Bcl6 resulted in increased expression of both Bcl2 and BCR. Given the positive correlation between the strength of T cell help and mTORC1 activity, our data suggest a model in which weak help from T cells together with provision of an increased survival signal are key for GC B cells to adopt a memory B cell fate.

Introduction

Memory B cells and long-lived plasma cells are responsible for effective long-term immunity against pathogens. The majority of these cells responding to T cell–dependent antigens are generated from the germinal center (GC) reaction. Indeed, memory B cells emerge from the GC as recirculating cells and, upon secondary antigen challenge, they are primed to elicit rapid antibody responses.

GCs are divided into two anatomical structures: the light zone (LZ) and the dark zone (DZ; Allen et al., 2007; Victora and Nussenzweig, 2012). B cells proliferate and undergo somatic hypermutation in the DZ before entering the LZ, where they exit the cell cycle. In the LZ, GC B cells expressing newly mutated B cell receptors (BCRs) capture antigen presented on follicular dendritic cells and internalize it for presentation to follicular helper T cells. Subsequently, antigen- and T cell–dependent selection takes place, whereby the "choice" of recycling to the DZ for further affinity maturation or of exiting the GC as plasma or memory B cells is made. In regard to the selection mechanism, it has been postulated that precursor cells destined to become recycling GC, plasma, or memory B cells already become committed in the LZ, at least to some extent, thereafter entering the recycling DZ, plasma, or memory B cell pools (Inoue et al., 2018). For instance, it has been demonstrated that a small fraction of LZ B cells expressing c-Myc, a key cell-cycle regulator, corresponds to precursor cells for the recycling GC fate; c-Myc^{+} cells are enriched for high-affinity BCRs and ablation of c-Myc affects DZ reentry (Calado et al., 2012; Dominguez-Sola et al., 2012; Finkin et al., 2019). Bcl6^{lo}CD69^{hi} LZ B cells expressing IRF4, a critical transcription factor for plasma cell differentiation, were recently shown to be the precursors of plasma cells (Ise et al., 2018).

In contrast to these insights into the precursor cells for recycling and plasma cell fates, studies of the memory fate decision have been hampered by the lack of a known master transcription factor for differentiation of memory B cells. Hence, surrogate markers such as an S1PR2 reporter, CCR6 expression, or a cell cycle reporter have been recently employed for identification of memory precursor cells (Laidlaw et al., 2017; Suan et al., 2017; Wang et al., 2017). Although informative, these studies have not identified key features for development of the

[1]Laboratory of Lymphocyte Differentiation, WPI Immunology Frontier Research Center, Osaka University, Osaka, Japan; [2]Medical Sciences Innovation Hub Program, RIKEN, Kanagawa, Japan; [3]Artificial Intelligence Medicine, Graduate School of Medicine, Chiba University, Chiba, Japan; [4]KOTAI Biotechnologies, Inc., Osaka, Japan; [5]Division of Cellular Therapy, Advanced Clinical Research Center, and Division of Stem Cell Signaling, Center for Stem Cell Biology and Regeneration Medicine, The Institute of Medical Science, The University of Tokyo, Tokyo, Japan; [6]Laboratory for Lymphocyte Differentiation, RIKEN Center for Integrative Medical Sciences, Kanagawa, Japan.

Correspondence to Tomohiro Kurosaki: kurosaki@ifrec.osaka-u.ac.jp.

GC-derived precursor cells committed to the long-lived memory B cell fate, or what signals regulate these key features.

Here, after identifying a memory-prone population ($CD38^{int}Bcl6^{hi/int}$ Ephrin-B1 [$Efnb1^{+}$]), we found that this small population exhibited lower mTORC1 activity than the recycling-prone population. Constitutive high mTORC1 activity led to defective development of $CD38^{int}Bcl6^{hi/int}Efnb1^{+}$ cells, whereas decreasing mTORC1 activity resulted in relative enrichment in this memory-prone cell population versus the recycling-prone one. Moreover, the $CD38^{int}Bcl6^{hi/int}Efnb1^{+}$ cells had higher levels of Bcl2 and surface BCR, thereby contributing to their survival and development. We also found that downregulation of Bcl6 resulted in increased expression of both Bcl2 and BCR. Given the positive correlation between the strength of T cell help and mTORC1 activity (Ersching et al., 2017), our data suggest a model in which weak help from T cells together with provision of an increased survival signal are key for GC cells to assume the memory B cell fate.

Results

Transition processes from GC to memory B cells

To clarify the initiating process for memory B cell differentiation occurring in the GC, we wished to identify GC B cells destined to the memory fate. For this, we used Bcl6 protein reporter mice (Kitano et al., 2011). We immunized these mice with 4-hydroxy-3-nitrophenylacetyl (NP)–chicken γ-globulin (CGG) in alum i.p. and analyzed NP-specific $IgG1^{+}$ splenic B cells at day 10. Since CD38 upregulation takes place during the transition from GC to memory B cells (Ridderstad and Tarlinton, 1998), we examined such $CD38^{+}$ B cells that still maintained GC identity to some extent, i.e., were $Bcl6^{+}$, together with conventional $CD38^{-}$ GC B cells. By using a fractionation method described previously (Fig. S1 A; Ise et al., 2018), the LZ B cells were further separated based on their Bcl6 and CD69 expression pattern (upper right panel in Fig. 1 A). Fraction (Fr.) 1 ($CD38^{-}Bcl6^{lo}CD69^{hi}$) and Fr.2 ($CD38^{-}Bcl6^{hi}CD69^{hi}$) cells are plasma and recycling GC precursor cells, respectively (Ise et al., 2018). Characterization of Fr.3 ($CD38^{-}Bcl6^{hi}CD69^{lo}$) cells is described below.

Efnb1 is expressed at a high level by almost all $Fas^{+}GL7^{+}$ cells, but is barely detectable on naive B cells (Laidlaw et al., 2017; Lu et al., 2017; Wang et al., 2017), allowing us to identify transitional populations between GC and memory B cells. Hence, for $CD38^{+}$ cells, by using Efnb1 and Bcl6, we further separated the $NP^{+}IgG1^{+}CD38^{+}GL7^{-}CD138^{-}$ cells into $Bcl6^{+}Efnb1^{+}$ (Fr.5), $Bcl6^{lo}Efnb1^{+}$ (Fr.6), and $Bcl6^{-}Efnb1^{-}$ (Fr.7; lower right panel in Fig. 1 A). Since expression level of Bcl6 in Fr.5 cells was slightly but significantly lower than that of Fr.3 cells, as shown by the left panel in Fig. 1 B, herein, we designated $Bcl6^{hi/int}$ for Fr.5. CD38 expression levels on Fr.5, Fr.6, and Fr.7 cells were increased in that order (middle panel in Fig. 1 B; herein, indicated as $CD38^{int}$, and $CD38^{+}$ for Fr.5 and 6/7, respectively). During the time course of the GC response, Fr.5 and Fr.6 cell numbers peaked at day 10 before declining, whereas Fr.7 cells peaked at day 12 and then slowly declined (Fig. S1 B). These kinetic data suggest that Fr.5 and Fr.6 contain cells that are transient and intermediate, and that once cells enter the Fr.7 pool, they are stably maintained. The Fr.7 cells displayed a typical $CD38^{+}Bcl6^{-}Efnb1^{-}$ mature memory phenotype (Fig. 1 B).

To assess the relationship between overall LZ B cells and Fr.5/6/7 cells, we performed RNA sequencing (RNA-seq) analysis (Fig. S2 A). To obtain sufficient amounts of RNA for this analysis, we used transferred $B1\text{-}8^{hi}$ B cells instead of non-BCR transgenic mice; these NP-specific transgenic GC B cells were present in similar proportions in each fraction as in non-BCR transgenic mice (Fig. S1 C). The principal component analysis (PCA) for each fraction indicated that memory B cells (Fr.7) clustered most tightly with $CD38^{+}Bcl6^{lo}Efnb1^{+}$ (Fr.6) cells but differed greatly from total LZ GC B cells (Fig. 1 C); Fr.5 cells were intermediate between Fr.6 and LZ GC B cells. Fr.6 cells expressed lower levels of *S1pr2* and higher levels of *Gpr183* (EBI2) mRNA compared with LZ B cells (Fig. S1 D), implying that they are a cell population in the process of exiting the GC; herein, we call Fr.6 "pre-memory B cells." In contrast to Fr.6 and mature memory B cells (Fr.7), Fr.5 cells seem to start the process of downregulating Bcl6. Fr.6 cells are most likely to correspond to the already identified GC-derived pre-memory B cells ("$Efnb1^{+}S1pr2^{lo}$ [Pop 4]"; Laidlaw et al., 2017), "LZ $CCR6^{+}$" (Suan et al., 2017), and "$mKO2^{hi}$" (Wang et al., 2017) in that, like those cells, Fr.6 cells are $Bcl6^{int/lo}Bach2^{int}$ (Fig. S3, A and B).

Fr.5 ($CD38^{int}Bcl6^{hi/int}Efnb1^{+}$) cells can be identified as pro-memory B cells

The above data prompted us to consider that, among Fr.2, Fr.3, and Fr.5 cells, the $CD38^{int}Bcl6^{hi/int}Efnb1^{+}$ cells (Fr.5) could be potential GC-derived precursors of the pre-memory B cells (Fr.6). To test this possibility, we took the following three approaches. First, PCA of the RNA-seq data was performed, indicating that $CD38^{int}Bcl6^{hi/int}Efnb1^{+}$ cells (Fr.5) and pre-memory B cells (Fr.6) clustered most closely together (Fig. 1 D). Second, to monitor cellular quiescence, we employed mVenus-$p27K^{-}$ transgenic mice, in which mainly G0 phase cells are labeled (Oki et al., 2014), demonstrating that in contrast to Fr.2 and Fr.3 cells, Fr.5 and Fr.6 cells had more mVenus-$p27K^{-}$ probe–positive, i.e., quiescent cells (Fig. 1 E). Finally, in order to assess the memory recall potential of the Fr.5 cells, we used a previously described adoptive transfer method (Wang et al., 2017). As illustrated in Fig. 1 F, Fr.2, Fr.3, Fr.5, or Fr.6 cells were isolated from NP-CGG/alum immunized mice and adoptively transferred (2×10^4 cells per mouse) into sublethally irradiated recipient mice together with $CD4^{+}$ T cells isolated from CGG-immunized mice. The recipient mice were then challenged with NP-CGG and analyzed on day 6 for NP-specific plasma cells. Although less proficient than pre-memory B cells (Fr.6), the ability of the adoptively transferred $CD38^{int}Bcl6^{hi/int}Efnb1^{+}$ (Fr.5) cells to give rise to plasma cells was significantly superior to Fr.2 and Fr.3 cells (Fig. 1 G). To rule out the possibility that Fr.5 cells were cells that had reentered the GC reaction from already generated memory B cells, we stained them for Ki67 and observed lower expression in Fr.5 than in the pre-GC B cells, which are in the process of entering the GC (Fig. S1 E). Together, $CD38^{int}Bcl6^{hi/int}Efnb1^{+}$ (Fr.5) cells are likely to be a precursor of pre-memory B cells, herein called Fr.5 "pro-memory B cells," and to represent a precursor population of previously identified

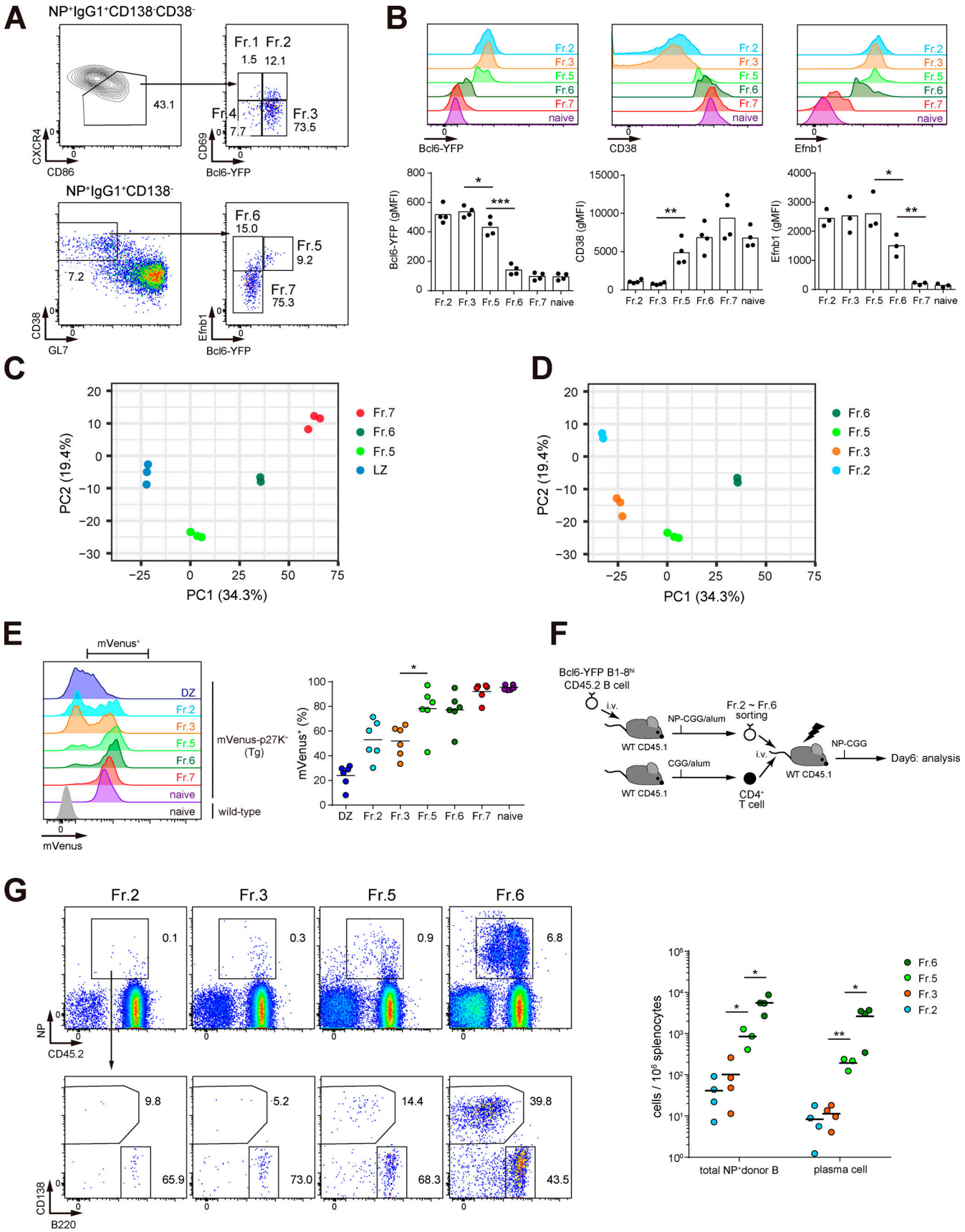

Figure 1. **Identification and characterization of pro-memory B cells. (A)** Flow cytometry gating for the analysis of splenocytes from Bcl6-YFP mice 10 d after i.p. immunization of NP-CGG/alum. See also Fig. S1 A for full gating strategy. **(B)** Top: Flow cytometry analysis of Bcl6-YFP, CD38, and Efnb1 expression in

each fraction and in naive B cells (B220$^+$CD38$^+$IgG1$^-$). Bottom: Cumulative data of geometric mean fluorescence intensity (gMFI). n = 4 (Bcl6-YFP and CD38), n = 3 (Efnb1), representative of two independent experiments. **(C)** PCA of RNA-seq data. Bcl6-YFP B1-8^{hi} naive B cells were transferred into wild-type CD45.1$^+$ mice. Mice were immunized i.p. with NP-CGG/alum and NP-specific IgG1$^+$ donor GC LZ, Fr.5, Fr.6, and Fr.7 B cells were sorted from nine pooled recipients on day 10 for one RNA-seq sample. See also Fig. S1 C for gating strategy. Each dot represents a single RNA-seq sample. n = 2 (Fr.6), n = 3 (LZ, Fr.5, Fr.7). **(D)** PCA of RNA-seq data. NP-specific IgG1$^+$ donor Fr.2, Fr.3, Fr.5, and Fr.6 B cells were sorted as in C. Each dot represents a single RNA-seq sample. n = 2 (Fr.2, Fr.6), n = 3 (Fr.3, Fr.5). **(E)** Left: Flow cytometry analysis of mVenus expression in each fraction in mVenus-p27K$^-$ transgenic mice 10 d after immunization with NP-CGG/alum, and in naive B cells in unimmunized wild-type mice. Right: Cumulative data of frequency of mVenus$^+$ cells in each fraction. n = 6, pooled from two independent experiments. **(F and G)** Recall potential of Fr.2, Fr.3, Fr.5, and Fr.6 cells. **(F)** Experimental design. Bcl6-YFP B1-8^{hi} naive B cells were transferred into wild-type mice and immunized with NP-CGG/alum. Each NP$^+$IgG1$^+$Fr. was sorted 10–12 d after immunization and transferred together with activated splenic CD4$^+$ T cells from CGG-immunized wild-type mice into sublethally irradiated wild-type mice, which were then rechallenged with NP-CGG. **(G)** Left: Flow cytometry analysis of CD45.1$^-$ donor splenocytes on day 6. Right: Cumulative data of number of total donor NP$^+$ B cells and NP$^+$ plasma cells (CD138$^+$B220^{lo}). n = 4 (Fr.2, Fr.3, Fr.6), n = 3 (Fr.5). Pooled from three independent experiments. *, P < 0.05; **, P < 0.01; ***, P < 0.001; unpaired Student's t test.

pre-memory B cells ("Efnb1$^+$*S1pr2*^{lo} [Pop 4]"; Laidlaw et al., 2017), "LZ CCR6$^+$" (Suan et al., 2017), and "mKO2^{hi}" (Wang et al., 2017; Fig. S3, A and B). However, we do not exclude the possibility that the pro-memory B cell population (Fr.5) is heterogeneous in its origins and properties; for instance, Fr.5 cells appear to overlap, to some extent, with LZ CCR6$^+$ cells in that they are beginning to express Ccr6 (Fig. S3 C).

Characterization of Fr.5 (CD38^{int}Bcl6$^{hi/int}$Efnb1$^+$) B cells

To gain insight into the specific features of CD38^{int}Bcl6$^{hi/int}$Efnb1$^+$ (Fr.5) cells that promote their potential development and/or differentiation into memory cells, we compared their RNA-seq profile to that of the other LZ B cells (Fr.2 and Fr.3; Fig. 2 A and Fig. S2 A); CD38$^-$Bcl6^{hi}CD69^{hi} (Fr.2) cells are destined to the recycling GC fate (Ise et al., 2018). Gene set enrichment analysis (GSEA) of Hallmark gene sets (Liberzon et al., 2015) revealed a strong enrichment in Fr.2 cells of c-Myc targets, E2F targets, and mTORC1 signaling genes (Fig. S4 A). Consistent with the mRNA analysis, expression of c-Myc protein, mTORC1 activity (assessed by phospho-S6), and E2F activity (assessed by phospho-Rb) were significantly decreased in Fr.5 cells (Fig. S4 B). In support of this, when we produced anti-NP IgH$_{V186.2}$ Igλ monoclonal antibodies cloned from single cell-sorted Fr.2 and Fr.5 NP$^+$IgG1$^+$ B cells and measured their relative affinity for NP$_{29}$- or NP$_1$-BSA, we found a significant overrepresentation of lower-affinity antibodies in CD38^{int}Bcl6$^{hi/int}$Efnb1$^+$ (Fr.5) cells (Fig. 2 B). Consistently, the frequency of canonical affinity–improving mutation (replacement of Trp33 with Leu33; W33L$^+$) was lower in Fr.5 cells (Fig. 2 C). Hence, we conclude that, in contrast to CD38$^-$Bcl6^{hi}CD69^{hi} (Fr.2) cells, most of the Fr.5 cells possess lower-affinity BCRs, an indication that they received less T cell help in the LZ (Victora et al., 2010).

We next compared the RNA-seq profile of Fr.3 to Fr.5 cells (Fig. 2 A and Fig. S2 A). Some differences were observed between these two fractions; particularly, expression of some of mTORC1 signaling genes was higher in Fr.3 than Fr.5 cells (Fig. 2 D). *Myc* expression in Fr.3 cells was somewhat higher compared with Fr.5 cells (Fig. 2 D). Reflecting these differences, GSEA showed an enrichment in Fr.3 of c-Myc targets and mTORC1 signaling genes (Fig. 2 E), although the enrichment extent of Fr.3 to Fr.5 was much smaller than Fr.2 to Fr.5 cells (Fig. S4 C). By flow cytometry analysis of c-Myc and pS6, however, we could not detect significant differences in both c-Myc protein expression and mTORC1 activity between Fr.3 and Fr.5 cells (Fig. S5 A). These data suggest that our flow cytometry analysis might not have sufficed to detect small changes induced by differential mRNA levels between Fr.3 and Fr.5 cells. An alternative possibility is that, in addition to mRNA level, changes in translational/posttranslational regulation might take place between Fr.3 and Fr.5 cells. The potential reason why Fr.5 but not Fr.3 cells can become pro-memory B cells, despite relatively small differences in RNA-seq profiles between these two populations, is described below.

Hyper-mTORC1 in Bach2/Blimp1 double-deficient GC cells

To identify key properties for the development of Fr.5 cells and/or their activity, we considered that Bach2/Blimp1 double-deficient GC B cells could provide a clue, since these mutant cells are defective in generating GC-derived memory B cells (Shinnakasu et al., 2016). To this end, we transferred B cells of three genotypes (*Bach2*$^{f/f}$*Prdm1*$^{f/f}$ERT2cre B1-8^{hi}, *Bach2*$^{+/+}$*Prdm1*$^{f/f}$ERT2cre B1-8^{hi}, and *Bach2*$^{+/+}$*Prdm1*$^{+/+}$ERT2cre B1-8^{hi}) into recipient mice, treated them with tamoxifen, and then immunized them with NP-CGG/alum (Fig. 3 A). In contrast to the control wild-type and Blimp1 single-deficient B cells, Bach2/Blimp1 double-deficient GC B cells showed an enrichment in DZ cells (Fig. 3 B). Moreover, the relatively small proportion of LZ B cells still contained Fr.2 and Fr.3 cells, whereas the numbers of Fr.5 and Fr.7 cells were robustly decreased in Bach2/Blimp1 double-deficient B cells (Fig. 3 B). Since Blimp1 single knockout did not significantly affect the numbers of pro-memory (Fr.5) and mature memory B cells (Fr.7; Fig. 3 B), we conclude that Bach2 plays an important role in development of pro-memory cells and subsequent mature memory B cells.

To determine how Bach2 participates in this process, we performed RNA profiling of Bach2/Blimp1 double-deficient LZ B cells, together with Blimp1-deficient LZ B cells as a control (Fig. S2 B). In Bach2/Blimp1 double-deficient LZ B cells, GSEA revealed a significant enrichment of c-Myc target genes, E2F target genes, and mTORC1 signaling genes, in that order (Fig. 3 C); this was also demonstrated by flow cytometry analysis (expression levels of c-Myc, pRb, and pS6; Fig. 3 D). Moreover, as expected, the mutant GC B cells were hyperproliferative, as assessed by 5-ethynyl-2′-deoxyuridine (EdU) pulse labeling (Fig. 3 E). These results, considering the previous demonstration that c-Myc–overexpressing and hyper-mTORC1 GC B cells manifest a bias toward the DZ (Ersching et al., 2017; Finkin et al., 2019), like Bach2/Blimp1 double-deficient GC B cells, allowed us to hypothesize that the defective pro-memory in the mutant GC cells

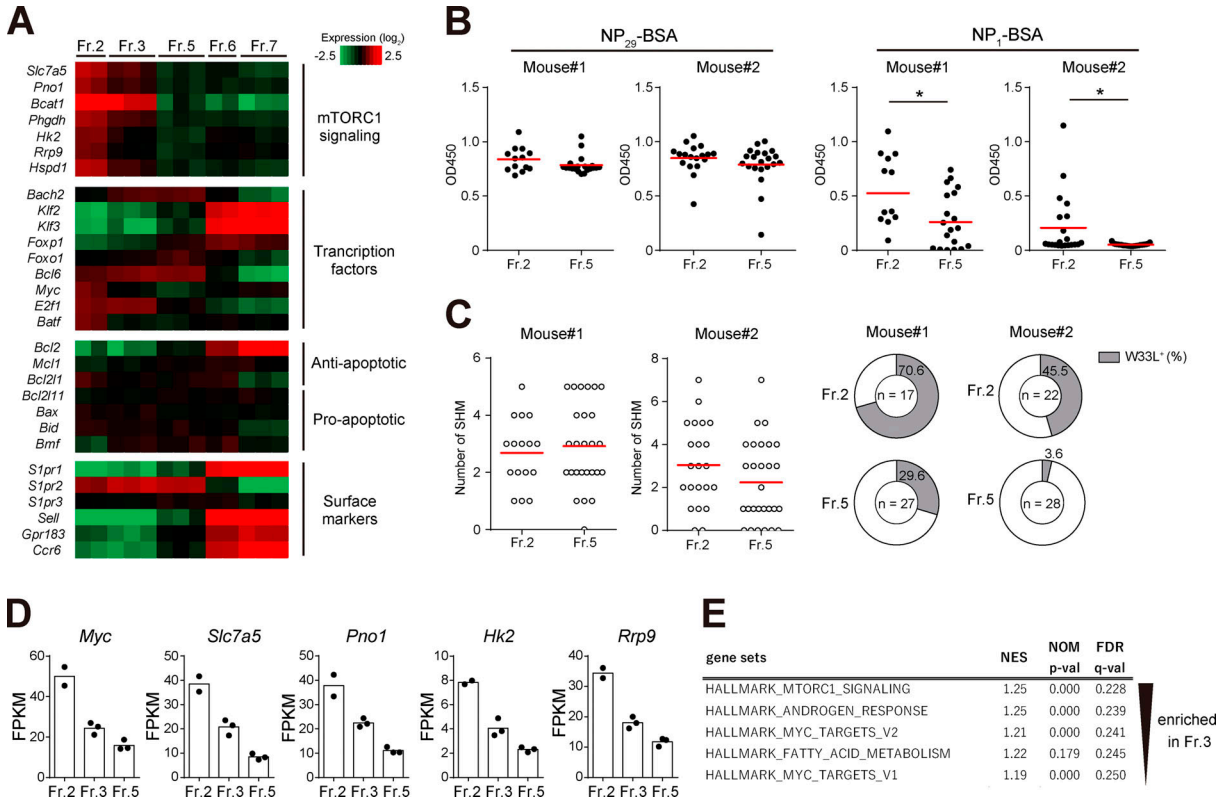

Figure 2. **Gene expression profiling and characterization of Fr.2, Fr.3, and Fr.5 cells. (A)** Heatmap of relative mRNA expression of selected genes in Fr.2, Fr.3, Fr.5, Fr.6, and Fr.7, grouped by gene ontology terms. Fragments per kilobase of exon per million reads mapped (FPKM) values in RNA-seq data (Fig. 1, C and D) are presented as $\log_2$ fold values, normalized by row. $n = 2$ (Fr.2, Fr.6), $n = 3$ (Fr.3, Fr.5, Fr.7). **(B)** Anti-NP affinity measurements by ELISA of monoclonal antibodies cloned from single cell–sorted IgG1$^+$NP$^+$ Fr.2 and Fr.5 cells from Bcl6-YFP mice 11 d after immunization with NP-CGG/alum. Each dot represents a single monoclonal antibody cloned from a single B cell. Results from two independent mice are shown. **(C)** Left: Numbers of somatic hypermutation (SHM) in cDNA of cloned monoclonal antibodies (B). Right: Pie charts showing the frequency of antibody clones containing W33L$^+$ mutation. Number in the center indicates total clones analyzed. **(D)** *Myc*, *Slc7a5*, *Pno1*, *Hk2*, and *Rrp9* mRNA expression presented as FPKM values in RNA-seq data (Fig. 1 D). Each dot represents a single RNA-seq sample. $n = 2$ (Fr.2, Fr.6), $n = 3$ (Fr.3, Fr.5, Fr.7). **(E)** GSEA of Fr.3 and Fr.5 RNA-seq data. All Hallmark gene sets enriched in Fr.3 or Fr.5 (false discovery rate q-value [q-val] < 0.25) were listed with normalized enrichment score (NES) and nominal (NOM) P value (p-val). *, $P < 0.05$; unpaired Student's *t* test.

5could result from anomalies of the mTORC1 and/or c-Myc pathways. Here, we focused our analysis on the mTORC1 pathway.

To test this hypothesis, we first asked whether normalizing mTORC1 activity in Bach2/Blimp1 double-deficient GC cells could rescue development of pro-memory B cells and subsequent memory B cells. We transferred *Bach2*$^{f/f}$*Prdm1*$^{f/f}$ERT2cre B1-8^{hi} B cells into rapamycin-resistant (*Mtor*$^{F2108L/F2108L}$) hosts (Ersching et al., 2017), deleted *Bach2* and *Prdm1* with tamoxifen, and then immunized the mice with NP-CGG/alum (Fig. 4 A). After immunization, the mice were treated with rapamycin to decrease mTORC1 activity in a transferred B cell–intrinsic manner. As shown in Fig. 4 B, the dose of rapamycin used nearly normalized pS6 levels in the Bach2/Blimp1 double-deficient LZ B cells. The rapamycin treatment partially corrected the c-Myc overexpression and hyperproliferation observed in the Bach2/Blimp1 double-deficient B1-8^{hi} B cells (Fig. 4 B), suggesting coexistence of mTORC1-dependent and -independent pathways to regulate c-Myc activities. In contrast to control vehicle treatment of Bach2/Blimp1 double-deficient B1-8^{hi} B cells, upon rapamycin treatment, those mutant cells generated threefold higher numbers of IgG1$^+$ memory B cells. The numbers of IgG1$^+$CD73$^+$ memory B cells were similarly increased (Fig. 4 C, right). Furthermore, the Fr.5:Fr.2 ratio was also increased upon rapamycin treatment (Fig. 4 D). However, the memory B cells number upon rapamycin treatment did not reach those from wild-type B1-8^{hi} B cells upon control vehicle injection (Fig. 4 C). Hence, we conclude that hyper-mTORC1 activity in Bach2/Blimp1 double-deficient GC B cells is one of the mechanisms that cause defective development of memory B cells, although there must be other, currently unknown ones, as well. In regard to GC B cells, the numbers were not significantly changed upon rapamycin treatment of Bach2/Blimp1 double-deficient B1-8^{hi} B cells. Skewing of Bach2/Blimp1 double-deficient GC B cells toward the DZ was decreased upon rapamycin treatment, although a small enrichment was still observed (Fig. 4 C).

Activity of mTORC1 regulates development of the Fr.5 pro-memory B cells

To further examine whether, in a wild-type setting, restraining mTORC1 activity could indeed facilitate differentiation of GC B cells to memory cells, we performed adoptive transfer

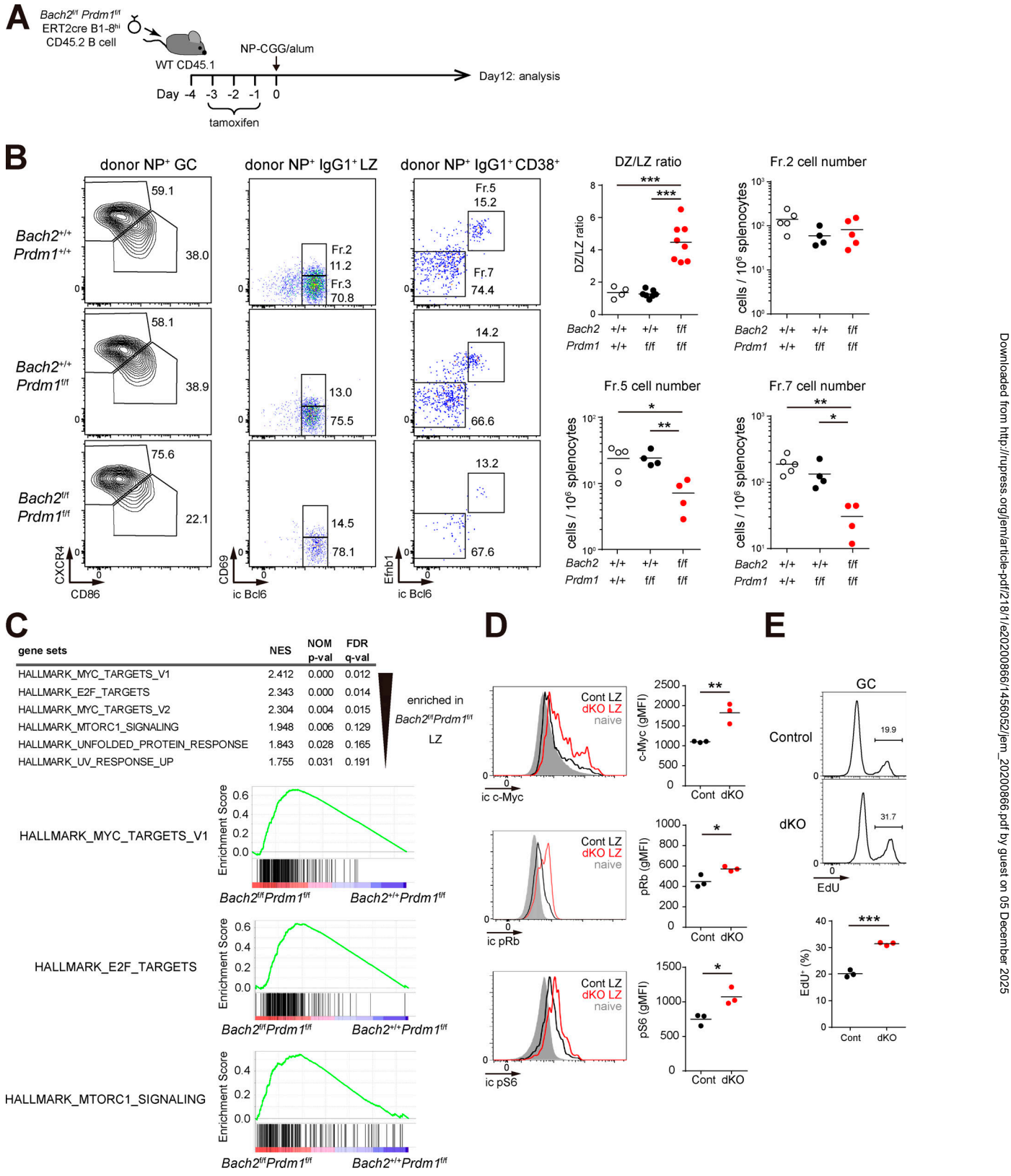

Figure 3. **Hyper mTORC1 activity in Bach2/Blimp1 double-deficient GC B cells. (A)** Experimental design of inducible Bach2 and Blimp1 double knockout (dKO) in the adoptive transfer experiment. *Bach2*$^{+/+}$*Prdm1*$^{+/+}$, *Bach2*$^{+/+}$*Prdm1*$^{f/f}$, or *Bach2*$^{f/f}$*Prdm1*$^{f/f}$ ERT2cre B1-8^{hi} naive B cells were independently transferred into wild-type CD45.1^{+} mice. Mice were administered with tamoxifen, immunized with NP-CGG/alum, and analyzed on day 12. **(B)** Left: Flow cytometry analysis of donor NP^{+} GC, donor NP^{+} IgG1^{+} LZ, and donor NP^{+} IgG1^{+} CD38^{+} cells. Right: Cumulative data of DZ:LZ ratio, and Fr.2, Fr.5, and Fr.7 cell numbers. *Bach2*$^{+/+}$*Prdm1*$^{+/+}$ and *Bach2*$^{f/f}$*Prdm1*$^{f/f}$ donor-derived NP^{+} IgG1^{+} GC B cell numbers are 4,206 ± 1,813 and 1,243 ± 374 cells per 10^6 splenocytes, constituted 48 ±

1.3% and 31 ± 3.3% among total recipient GC B cells, respectively. n = 4 ($Bach2^{+/+}Prdm1^{+/+}$), n = 7 ($Bach2^{+/+}Prdm1^{f/f}$), n = 8 ($Bach2^{f/f}Prdm1^{f/f}$) for DZ:LZ ratio, pooled from four independent experiments. n = 5 ($Bach2^{+/+}Prdm1^{+/+}$), n = 4 ($Bach2^{+/+}Prdm1^{f/f}$, $Bach2^{f/f}Prdm1^{f/f}$) for cell number. Representative of two independent experiments. **(C)** GSEA of RNA-seq data from LZ B cells. $Bach2^{+/+}Prdm1^{f/f}$, or $Bach2^{f/f}Prdm1^{f/f}$ ERT2cre B1-8^{hi} naive B cells were independently transferred into wild-type CD45.1$^+$ mice. Mice were administered with tamoxifen and immunized with NP-CGG/alum. NP-specific donor GC LZ and DZ B cells were sorted from five pooled recipients on day 10 for one RNA-seq sample. See also Fig. S2 B for heatmap of the top 50 differentially expressed genes. n = 2 for each population. Gene sets with false discovery rate (FDR) q-value (q-val) < 0.25 are shown in the table. **(D)** Left: Flow cytometry analysis of intracellular (ic) expression of c-Myc, pRb, and pS6 in control (Cont; $Bach2^{+/+}Prdm1^{+/+}$ or $Bach2^{+/+}Prdm1^{f/f}$) LZ, dKO ($Bach2^{f/f}Prdm1^{f/f}$) LZ, and wild-type naive B cells. Right: Cumulative data of geometric mean fluorescence intensity (gMFI). n = 3, representative of two independent experiments. **(E)** Top: Flow cytometry analysis of pulse-labeled EdU incorporation in control ($Bach2^{+/+}Prdm1^{+/+}$ or $Bach2^{+/+}Prdm1^{f/f}$) and dKO ($Bach2^{f/f}Prdm1^{f/f}$) GC B cells. Bottom: Cumulative data of EdU$^+$ ratio. n = 3, representative of two independent experiments. *, P < 0.05; **, P < 0.01; ***, P < 0.001; unpaired Student's t test.

experiments. For this, we conducted experiments in which two types of congenically marked B cells, rapamycin-sensitive ($Mtor^{+/+}$) and rapamycin-resistant ($Mtor^{F2108L/F2108L}$) B1-8^{ge} B cells, were cotransferred as a 1:1 mixture into rapamycin-resistant hosts ($Mtor^{F2108L/F2108L}$), which were immunized with NP-CGG/alum and then administered with rapamycin. As expected, rapamycin treatment led to a decrease in S6 phosphorylation in the transferred rapamycin-sensitive, but not

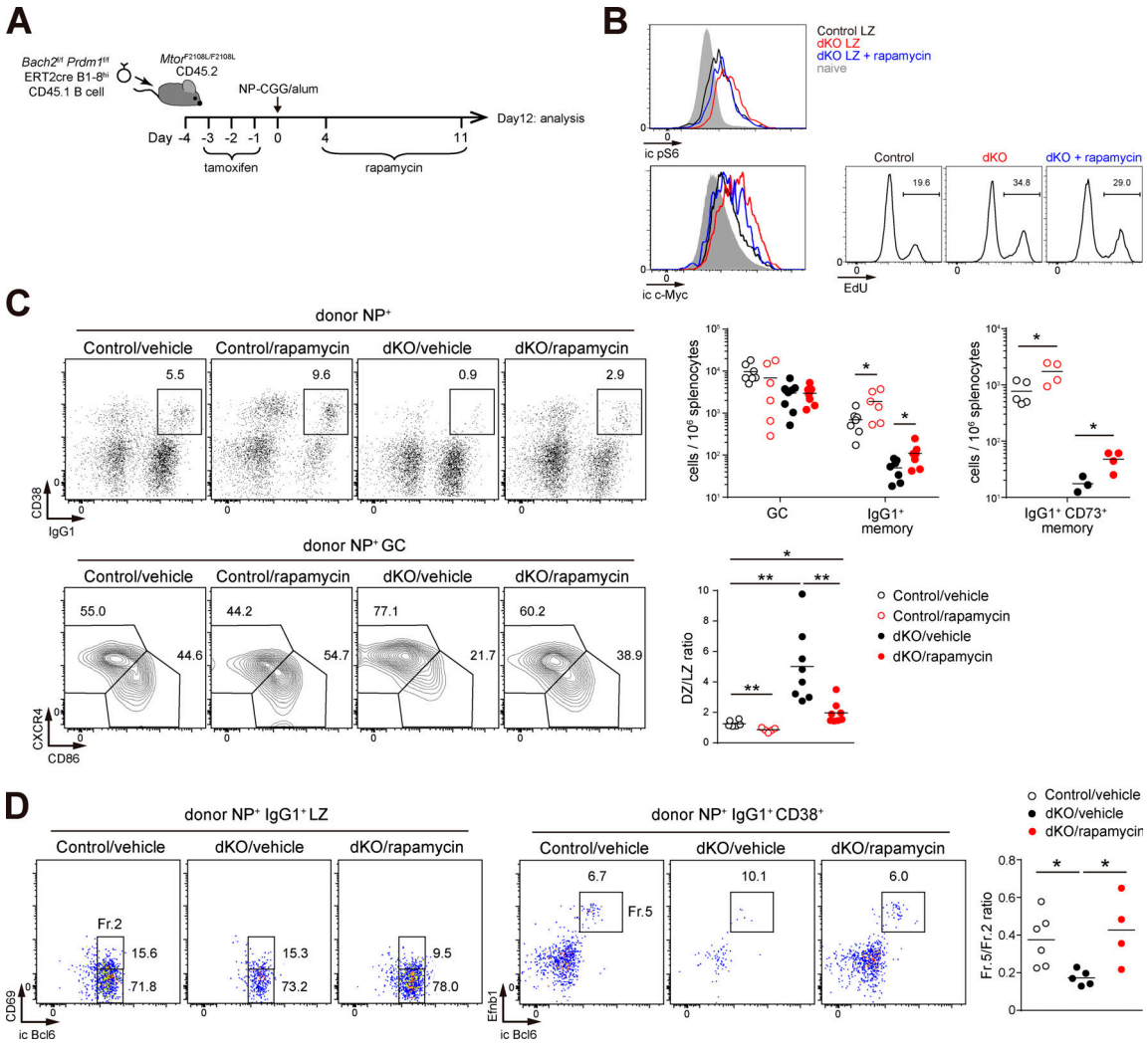

Figure 4. **Partial rescue of memory B cell generation by rapamycin treatment in Bach2/Blimp1 double-deficient GC B cells. (A)** Experimental design of B cell–specific rapamycin treatment using Bach2 and Blimp1 double-deficient B cells. Control ($Bach2^{+/+}Prdm1^{+/+}$) or double knockout (dKO; $Bach2^{f/f}Prdm1^{f/f}$) ERT2cre B1-8^{hi} CD45.1$^+$ naive B cells were independently transferred into wild-type mice. Mice were administered with tamoxifen, immunized with NP-CGG/alum, injected with rapamycin daily during days 4–11, and analyzed on day 12. **(B)** Flow cytometry analysis of intracellular (ic) expression of pS6 and c-Myc in control LZ, dKO LZ, and wild-type naive B cells (left), and pulse-labeled EdU incorporation in control and dKO GC B cells (right). Representative of three independent experiments. **(C)** Left: Flow cytometry analysis of donor NP$^+$ and donor NP$^+$ GC B cells. Right: Cumulative data of GC, IgG1$^+$ memory, and IgG1$^+$ CD73$^+$ memory B cell number, and DZ:LZ ratio. n = 6–8 for GC and IgG1$^+$ memory B cell number and DZ:LZ ratio, n = 3–5 for IgG1$^+$ CD73$^+$ memory B cell number. Pooled from two independent experiments. **(D)** Left: Flow cytometry analysis of donor NP$^+$IgG1$^+$ LZ and donor NP$^+$IgG1$^+$CD38$^+$ B cells. Right: Cumulative data for the Fr.5:Fr.2 ratio. n = 4–6, representative of two independent experiments. *, P < 0.05; **, P < 0.01; unpaired Student's t test.

rapamycin-resistant, B1-8^{ge} GC B cells (Fig. 5 A). Upon rapamycin treatment, the number of rapamycin-sensitive NP^{+} GC B cells was decreased while the number of NP^{+} memory B cells was increased compared with their rapamycin-resistant counterparts, assessed by conventional flow cytometry analysis (Fig. 5 B). To more directly demonstrate the transition from GC B cells to Fr.7 cells, we treated the immunized mice with EdU for 3 d (days 10–13) before analysis. In this setting, incorporation of EdU marks GC cells that divided during the treatment period and the resultant quiescent memory B cells (Fig. 5 C). We previously confirmed that during this period, the majority of proliferating cells (>95%) are GC B cells and plasmablasts (Shinnakasu et al., 2016). Upon rapamycin treatment, the frequency of EdU^{+}IgG1^{+} Fr.7 cells compared with GC cells was higher among the rapamycin-sensitive B1-8^{ge} cells than the rapamycin-resistant ones, demonstrating rapamycin-mediated facilitation of the transition from GC to Fr.7 cells (Fig. 5 D). Moreover, upon rapamycin treatment, the numbers of CD38^{-}Bcl6^{hi}CD69^{hi} (Fr.2) and CD38^{int}Bcl6$^{hi/int}$Efnb1^{+} (Fr.5) rapamycin-sensitive B1-8^{ge} IgG1^{+} B cells were decreased and maintained, respectively. Thus, the ratio of Fr.5 to Fr.2 was increased (Fig. 5 E). Together, we conclude that a relative enrichment in Fr.5 over Fr.2 cells is induced by rapamycin treatment, thereby facilitating the overall transition from GC B cells to memory B cells. The memory B cells generated in the presence of rapamycin were able to induce similar recall antibody responses to those generated in the absence of rapamycin, as assessed by adoptive transfer experiments (Fig. 5 F).

Expression of Bcl2 and surface BCR are upregulated during differentiation toward mature memory B cells

We next wished to examine why Fr.5, but not Fr.3 cells, can become pro-memory B cells. Since there were almost no differences in mTORC1 activity between Fr.5 and Fr.3 cells (Fig. S5 A), it appears that an mTORC1^{lo} state is necessary but not sufficient for development of pro-memory B cells (Fr.5); thus, additional key properties must be required for development of these cells. Since one of crucial features of mature memory B cells is longevity, one straightforward possibility is that Fr.5 cells begin to acquire more survival activity. Supporting this idea, CD38^{int}Bcl6$^{hi/int}$Efnb1^{+} (Fr.5) cells were less apoptotic compared with CD38^{-}Bcl6^{hi}CD69^{lo} (Fr.3) cells as assessed by active caspase-3 staining (Fig. 6 A). Transcript data (Fig. 6 B) together with protein expression data (Fig. 6 C) demonstrated that Bcl2 expression was upregulated in Fr.5 cells compared with Fr.3 cells, and even more in pre-memory B cells (Fr.6). Similarly, we found that the cell surface BCR expression level was increased stepwise from Fr.3 to Fr.6 cells (Fig. 6 D). We also observed a slight increase of IgG1 and Igα/β mRNA expression in Fr.5 over Fr.3 cells; thus, regulation of both mRNA and protein levels seems to be operative.

To examine whether Bcl2 family protein–mediated survival activity could impact the development of Fr.5 cells, we employed GC B cells with haploinsufficiency of Bim (*Bcl2l11*; see Materials and methods), a counteracting factor against anti-apoptotic Bcl2-family members (O'Connor et al., 1998). *Bcl2l11*$^{+/+}$ ERT2cre B1-8^{ge} B cells and *Bcl2l11*$^{f/+}$ERT2cre B1-8^{ge} B cells were cotransferred as a 1:1 mixture into wild-type recipient mice, which were then immunized with NP-CGG/alum and treated with tamoxifen on day 8 (Fig. 6 E). Bim mRNA expression was decreased to almost 50% of control levels after tamoxifen treatment in *Bcl2l11*$^{f/+}$ GC B cells (Fig. 6 F). In this competitive setting, among the Fr.2/3/5/6 cells, the frequency was most significantly increased in Fr.5 and Fr.6 cells upon Bim haploinsufficiency (Fig. 6 G), although there was also a modest increase of Fr.3 cells. Consequently, the frequency of *Bcl2l11*$^{f/+}$ NP^{+}IgG1^{+}CD73^{+} memory B cells was also increased (Fig. S5 B).

To examine the effects of surface BCR expression on survival, B1-8$^{ge\text{-}flox/+}$ ERT2cre B cells were employed. For these particular experiments, we mixed these B cells and control B1-8$^{ge/+}$ ERT2cre B cells at a 7:3 ratio and adoptively cotransferred them into recipient mice, which were then immunized with NP-CGG/alum (Fig. 6 H). We injected tamoxifen on day 10 and examined surface BCR expression on day 12, demonstrating a significant decrease on Fr.5 cells derived from B1-8$^{ge\text{-}flox/+}$ ERT2cre B cells (Fig. 6 I). To detect apoptotic cells in this experiment, we analyzed mixtures of Fr.5 and Fr.6 cells (CD38^{+}Efnb1^{+}) to acquire a sufficient number of cells for the assay. As demonstrated in Fig. 6 J, concomitant with decreased surface BCR expression, there was a higher frequency of apoptotic (aCasp3^{+}) cells among pro/pre-memory cells derived from B1-8$^{ge\text{-}flox/+}$ ERT2cre B cells. Similarly, frequency of apoptotic cells among total LZ GC cells was enhanced upon BCR downregulation (Fig. S5 C). A control experiment using *Prdm1*$^{f/+}$B1-8$^{ge/+}$ ERT2cre B cells showed that a nonspecific effect on apoptosis induced simply by Cre-mediated double-strand breaks was negligible (Fig. S5 D). Together, stepwise increases of Bcl2 and surface BCR expression from pro-memory (Fr.5) cells to pre-memory (Fr.6) toward mature memory B cells are likely to contribute to their survival.

Downregulation of Bcl6 affects the level of Bcl2 and surface BCR

We next sought to identify a potential mechanism for upregulation of Bcl2 and BCR in the CD38^{int}Bcl6$^{hi/int}$Efnb1^{+} (Fr.5) cells. Given the previous evidence that Bcl6 suppresses Bcl2 expression (Saito et al., 2009), we reasoned that the onset of Bcl6 downregulation in Fr.5 might be involved. To examine this possibility, *Bcl6*$^{+/+}$ ERT2cre B1-8^{ge} B cells and *Bcl6*$^{f/+}$ ERT2cre B1-8^{ge} B cells were cotransferred as a 1:1 mixture into wild-type recipient mice, which were immunized with NP-CGG/alum and treated with tamoxifen (Fig. 7 A). *Bcl6* mRNA expression was decreased to ∼55% of control cells on day 12 in *Bcl6*$^{f/+}$ LZ B cells (Fig. 7 B), and this was accompanied by a significant increment of Bcl2 mRNA and surface BCR expression (Fig. 7, B and C). IgG1 and Igα/β mRNA expression was comparable between *Bcl6*$^{+/+}$ and *Bcl6*$^{f/+}$ LZ B cells (Fig. 7 B). Thus, the regulation of mRNA or proteins seems to be dominantly operative in the case of Bcl2 or surface BCR, respectively. These data suggest that downregulation of Bcl6 is able to confer a Fr.5 cell–like phenotype on LZ B cells in regard to expression of Bcl2 and surface BCR. Since Bcl6 was genetically altered in these experiments, it was difficult to employ Bcl6 as a marker to distinguish between Fr.1 and Fr.2 and between Fr.5 and Fr.6 (Fig. 1 A). Therefore, we characterized mixtures of Fr.1 and Fr.2 (precursors

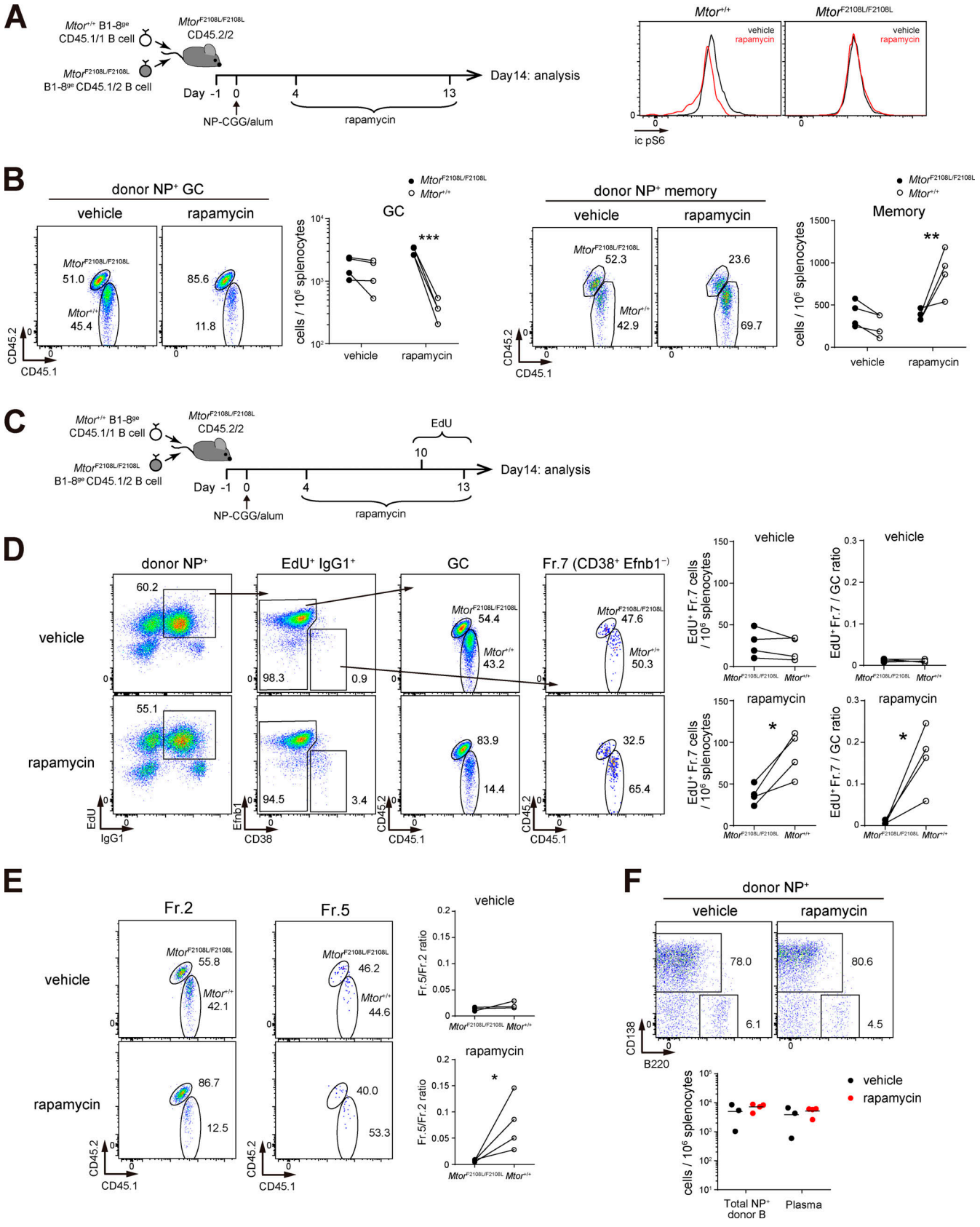

Figure 5. **Lower mTORC1 activity in GC B cells favors the memory fate. (A)** Left: Experimental design of competitive cotransfer of rapamycin-sensitive and -resistant B1-8^{ge} B cells. Congenically marked *Mtor*$^{+/+}$ and *Mtor*$^{F2108L/F2108L}$ B1-8^{ge} naive B cells were cotransferred as a 1:1 mixture into *Mtor*$^{F2108L/F2108L}$ hosts, which were immunized with NP-CGG/alum, administered with rapamycin daily during day 4–13, and analyzed on day 14. Right: Flow cytometry analysis of

intracellular (ic) expression of pS6 in *Mtor*$^{+/+}$ or *Mtor*$^{F2108L/F2108L}$ LZ B cells with or without rapamycin treatment. Representative of three independent experiments. **(B)** Flow cytometry analysis and cumulative data of donor NP$^+$ GC (left) and donor NP$^+$ memory B cells (right). *n* = 4, representative of two independent experiments. **(C)** Experimental design of competitive cotransfer of rapamycin-sensitive and -resistant B1-8^{ge} B cells with EdU labeling. Mice were prepared as in A, and proliferative GC-derived cells were labeled with EdU (injected i.p. on day 10 and then in the drinking water during days 10–13). **(D)** Left: Flow cytometry of donor NP$^+$ cells prepared as in C. Right: Cumulative data of EdU$^+$ Fr.7 memory B cell number and EdU$^+$ Fr.7:GC ratio. *n* = 4, representative of two independent experiments. **(E)** Left: Flow cytometry of Fr.2 and Fr.5 cells prepared as in C. Right: Cumulative data of Fr.5:Fr.2 ratio. *n* = 4, representative of two independent experiments. **(F)** Recall potential of IgG1$^+$ memory B cells generated after rapamycin treatment. B1-8^{ge} B cells were transferred into *Mtor*^{F2108L} recipient mice. After immunization with NP-CGG/alum, mice were treated with or without rapamycin as in C, and NP$^+$ IgG1$^+$ memory B cells were sorted on day 14. Adoptive transfer with activated CD4$^+$ T cells was performed as in Fig. 1 F. On day 6 after a boost with NP-CGG, donor NP$^+$ splenocytes were analyzed by flow cytometry (top), and donor NP$^+$ B cells and donor NP$^+$ plasma cells were quantified (bottom). *n* = 3 (vehicle), *n* = 4 (rapamycin), pooled from three independent experiments. *, P < 0.05; **, P < 0.01; ***, P < 0.001; paired Student's *t* test.

for plasmablasts and recycling GCs) as CD69$^+$ LZ B cells and those of Fr.5 and Fr.6 (including pro-memory and pre-memory cells) as CD38$^+$Efnb1$^+$ B cells, demonstrating that the CD38$^+$Efnb1$^+$:CD69$^+$ LZ ratio is increased in *Bcl6*$^{f/+}$ ERT2cre B1-8^{ge} B cells (Fig. 7 D). We also found a significant increase of *Bcl6*$^{f/+}$ NP$^+$IgG1$^+$CD73$^+$ memory B cells compared with their *Bcl6*$^{+/+}$ counterparts (Fig. 7 E). Collectively, these data suggest that downregulation of Bcl6 is one of the potential mechanisms to upregulate Bcl2 and surface BCR in pro/pre-memory B cells, possibly contributing to memory B cell development.

Discussion

It is still unclear what signals and processes in LZ GC cells initiate their differentiation toward long-lived memory B cells. Here, by focusing on key features for development of GC-derived memory precursors, we show that an mTORC1^{lo} state is necessary to develop pro-memory B cells. Since mTORC1^{lo} LZ B cells receive weak T cell help and, as a result, have been thought to undergo apoptosis, this raises the question of how such pro-memory B cells are prevented from dying and able to differentiate into mature memory B cells. Our experiments suggest that the memory precursor B cells express higher levels of Bcl2 and surface BCR, thereby acquiring a survival advantage.

We have already shown that Bach2^{hi} LZ GC B cells are predisposed to differentiate into memory B cells (Shinnakasu et al., 2016), indicating that memory cell commitment already begins in a subset of GC B cells. This memory-prone subset most likely corresponds to the Fr.5 (CD38^{int}Bcl6$^{hi/int}$Efnb1$^+$ pro-memory) cells; indeed, expression of Bach2 in Fr.5 is higher than in Fr.2 cells (Fig. 2 A and Fig. S3 B). Fr.6 (pre-memory B) cells appear to be undergoing a further developmental step toward mature memory B cells, manifested by further downregulation of Bcl6 (Fig. 1 B). We found that mTORC1 has a marked effect on the ratio of memory-prone (Fr.5) to recycling-prone (Fr.2) GC B cell formation. Rapamycin treatment increased the proportion of Fr.5 cells and, conversely, hyperactivation of mTORC1 in the Bach2/Blimp1 double-deficient setting led to a relative increase in Fr.2 cells.

Several nonmutually exclusive possibilities can be envisaged to explain why lower mTORC1 activity contributes to development of memory-prone cells. Decay in mTORC1 activity as GC B cells proliferate in the DZ appears to be required for their timely return to the LZ (Ersching et al., 2017). Given the importance of LZ residency for memory differentiation (Bannard et al., 2013), one possibility is that LZ residency imposed by mTORC1^{lo} could allow development of pro-memory B cells. Second, apart from this spatial requirement mediated through modulation of mTORC1, inhibition of mTORC1, as is seen during the generation of natural killer cell memory (O'Sullivan et al., 2015), may stimulate autophagy, thereby enhancing pro-memory B cell survival. Finally, it is also well known that mTORC1 activity is suppressed in memory B cells (Boothby and Rickert, 2017). Such metabolic changes as the cells progress toward mature memory B cells thus appear to be initiated already in pro-memory cells, and this might be a necessary first step for generating mature memory B cells.

The partial restoration of memory B cells by rapamycin treatment in Bach2/Blimp1 double-deficient GC cells suggests that, in addition to hyper-mTORC1 activity, other anomalies occur in mutant GC B cells in regard to memory differentiation. One of them is likely the c-Myc overexpression, because of the following. First, indeed, in rapamycin-treated Bach2/Blimp1 double-deficient GC cells, overexpression of c-Myc and hyperproliferation were still observed to a significant extent (Fig. 4 B). Second, c-Myc–overexpressing GC cells were reported to have a significant bias toward the DZ (Finkin et al., 2019). Considering the importance of LZ residency for memory differentiation (Bannard et al., 2013), overexpression of c-Myc is assumed to be detrimental to memory differentiation. Hence, we would propose that restraining both mTORC1-mediated metabolism and c-Myc–mediated cell-cycle progression is required to develop pro-memory B cells and that Bach2 is one of the critical regulators for suppressing both pathways.

Functionally, Bach2 is well known to act as a repressive guardian transcription factor (Igarashi et al., 2017). In regard to relationship between signaling and Bach2 expression, the mTORC1 activity and Bach2 expression appear to be mutually exclusive, because the BCR-induced AKT-mTORC1 inhibits Bach2 expression (Kometani et al., 2013), and Bach2 represses transcription of mTORC1 signaling molecules. Such a negative feedback loop is characteristic of "bistable" signal transduction circuits, which can operate in two stable formats. This might take place between Fr.5 and Fr.2 cells. It should be mentioned that, from mTORC1 signaling molecule side, Bach2 is one of the transcription factors, and probably additional factors participate in transcriptional regulation on mTORC1 signaling genes. In addition to the connection between BCR signal and Bach2, considering the T cell data showing that ICOS and integrin αE are upregulated in Bach2^{lo} T cells (Grant et al., 2020; Sidwell

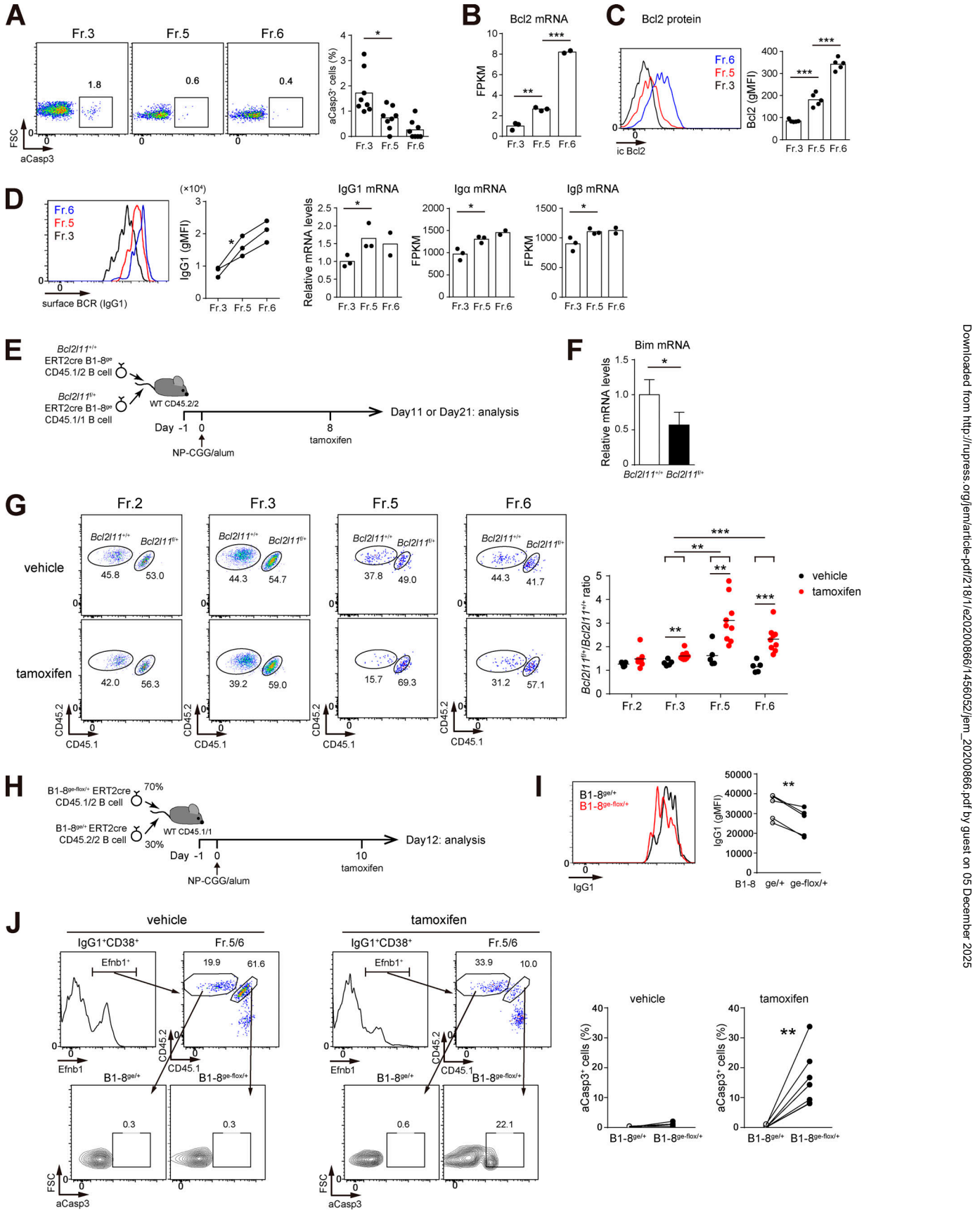

Figure 6. **Survival advantage of pro-memory B cells over Fr.3 cells. (A)** Left: Flow cytometry analysis of active caspase-3 (aCasp3) staining in Fr.3, Fr.5, and Fr.6 cells. Bcl6-YFP B1-8^{hi} naive B cells were transferred into wild-type CD45.1^{+} mice, which were immunized with NP-CGG/alum and analyzed on day 11. Right:

Cumulative data of aCasp3$^+$ ratio. n = 8, pooled from three independent experiments. **(B)** *Bcl2* mRNA expression presented as fragments per kilobase of exon per million reads mapped (FPKM) values in RNA-seq data (Fig. 1, C and D). Each dot represents single RNA-seq sample. n = 3 (Fr.3, Fr.5), n = 2 (Fr.6). **(C)** Left: Flow cytometry analysis of intracellular (ic) Bcl2 expression in Fr.3, Fr.5, and Fr.6 cells prepared as in A. Right: Cumulative data of geometric mean fluorescence intensity (gMFI). n = 5, representative of two independent experiments. **(D)** Far left: Flow cytometry analysis of surface IgG1 expression in Fr.3, Fr.5, and Fr.6 cells prepared as in A. Second from left: Cumulative data of IgG1 gMFI. n = 3, representative of two independent experiments. Middle: Relative IgG1 mRNA expression determined by real-time qPCR analysis. Second from right and far right: Igα and Igβ mRNA expression presented as FPKM values in RNA-seq data (Fig. 1 D), respectively. Each dot represents a single RNA-seq sample. n = 3 (Fr.3, Fr.5), n = 2 (Fr.6). **(E–G)** Assessment of the effect of inducible Bim haploinsufficiency in GC B cells on memory B cell generation. **(E)** Experimental protocol. Congenically marked *Bcl2l11*$^{+/+}$ and *Bcl2l11*$^{f/+}$ ERT2cre B1-8^{ge} naive B cells were cotransferred as a 1:1 mixture into wild-type mice, which were immunized with NP-CGG/alum, administered with tamoxifen on day 8, and analyzed on day 11. **(F)** Relative Bim mRNA expression in LZ B cells determined by real-time qPCR analysis. n = 4 (*Bcl2l11*$^{+/+}$), n = 3 (*Bcl2l11*$^{f/+}$). **(G)** Left: Flow cytometry analysis of Fr.2, Fr.3, Fr.5, and Fr.6 cells. Right: Cumulative data of *Bcl2l11*$^{f/+}$:*Bcl2l11*$^{+/+}$ ratio. n = 5 (vehicle), n = 9 (tamoxifen), pooled from two independent experiments. **(H–J)** Assessment of the effect of inducible BCR deletion on pro-memory B cells. **(H)** Experimental protocol. Congenically marked B1-8$^{ge\text{-}flox/+}$ and B1-8$^{ge/+}$ ERT2cre naive B cells were cotransferred as a 7:3 mixture into wild-type CD45.1/1 mice, which were immunized with NP-CGG/alum, administered with tamoxifen on day 10, and analyzed on day 12. **(I)** Left: Flow cytometry analysis of surface IgG1 expression in Fr.5 cells. Right: Cumulative data of gMFI. n = 5, pooled from two independent experiments. **(J)** Left: Flow cytometry analysis of donor IgG1$^+$CD38$^+$ B cells. Right: Cumulative data of aCasp3$^+$ ratio. n = 4 (vehicle), n = 7 (tamoxifen), pooled from two independent experiments. *, P < 0.05; **, P < 0.01; ***, P < 0.001; unpaired Student's t test (A–D middle, second from right, far right, F, and G) and *, P < 0.05; **, P < 0.01; paired Student's t test (D second from left, I, and J). FSC, forward scatter.

et al., 2020), Bach2 might be involved in connecting the BCR signal to T cell help. For instance, Bach2^{lo} LZ GC cells with high-affinity BCRs might modulate T/B interactions through adhesion status and coreceptor expression and affect the strength of T cell help. This might further downregulate Bach2, because we previously showed that strong T cell help depresses Bach2 expression (Shinnakasu et al., 2016).

After moving back into the LZ, apoptosis is generally thought to be the default pathway for LZ GC B cells; however, high-affinity cells are spared and positively selected after they encounter sufficient cognate T cell help (Allen et al., 2007; Victora and Nussenzweig, 2012). These spared high-affinity cells correspond to Fr.2 cells, whereas the defaulting apoptotic LZ cells are likely to be Fr.3 cells; indeed, among LZ GC cells, Fr.3 cells were most apoptotic. Here, we show that a small population of pro-memory B cells exists in the LZ and, despite apparently receiving weak T cell help, they are relatively resistant to apoptosis. The inability of prior studies to detect such apoptosis-resistant LZ B cells is most likely due to the fact that the numbers of pro-memory cells are so limited (Mayer et al., 2017).

Previous data using B cell–specific Bcl2-tg mice (Smith et al., 1994) or Bim knockout mice (Fischer et al., 2007) showed that such mice develop an enlarged memory B cell compartment. Recently, more detailed analysis using the same Bcl2-tg mice (Stewart et al., 2018) provided mechanistic insights into the above phenomenon. First, in these mice, aberrant populations of seemingly quiescent cells arise that express markers of memory precursor cells. Second, overexpression of Bcl2 is not sufficient for DZ GC B cells with damaged BCRs to reach the LZ. Hence, in a physiological setting, it is reasonable to speculate that, after returning to the LZ in a Bcl2-independent manner, if Bcl2 expression is upregulated in some of the LZ GC B cells, they are better able to be rescued from apoptosis in the late G1 phase and to begin to differentiate into memory B cells. Supporting this idea, we show here that among LZ GC cells, small numbers of pro-memory B cells (Fr.5), but not Fr.3 cells, begin to upregulate Bcl2, and that development of pro-memory B cells is facilitated by Bim haploinsufficiency. Because Bach2 expression in Fr.5 cells is similar to Fr.3 cells (Fig. S3 B), Bach2 appears not to be involved in such differential survival activity between Fr.5 and Fr.3 cells. Rather, a Bach2-independent mechanism such as Bcl6 downregulation (discussed below) is likely to be operated, thereby allowing Fr.5 cells to survive enough to begin to differentiate into memory precursor cells. In contrast to Fr.5 cells (pro-memory), Fr.6 cells (pre-memory) apparently possess more survival activity (Fig. 6 A), possibly explaining the generation kinetics between Fr.5 and Fr.6 cells; Fr.6 cells were more accumulated at later phases (days 14 and 20) during immune responses (Fig. S1 B).

Induced downregulation of surface BCR expression in pro/pre-memory B cells resulted in increased apoptosis in the pro-memory B cells. These results, together with the evidence that pro-memory B cells express higher surface BCR levels, lead us to propose that the BCR-mediated survival signal also plays a role in the development of pro-memory B cells. Based on the previous report that BCR ablation leads to cell death, which can be delayed by constitutive Bcl2 expression (Lam et al., 1997), we considered the possibility that downregulation of the BCR might decrease Bcl2 expression in pro/pre-memory B cells. However, we could not detect such a connection (data not shown). In naive B cells, the constitutive PI3 kinase–Foxo1 pathway is known to replace the missing BCR-mediated survival signals (Srinivasan et al., 2009). Therefore, a question arises of how pro-memory B cells, despite being mTORC1^{lo} (reflecting lower Akt activity), generate such a survival signal. Given that there is no enlarged GC phenotype in PTEN or Foxo1 knockout mice (Dominguez-Sola et al., 2015; Inoue et al., 2017; Sander et al., 2015; Suzuki et al., 2003), one straightforward explanation might be that the quality and/or quantity of BCR-mediated survival signals differ between naive B cells and GC-derived memory B cells.

We provide evidence that downregulation of Bcl6 in pro-memory B cells could be one of the mechanisms for upregulation of Bcl2 and surface BCR. However, since the extent of Bcl6 downregulation in pro-memory B cells is small, such a slight change might not account for the observed upregulation of Bcl2 and surface BCR. Hence, our data cannot completely exclude the possibility that, particularly at the pro-memory B cell stage, other mechanisms might operate to initiate upregulation of Bcl2 and BCR. In this case, it is likely that downregulation of Bcl6 acts as an amplification pathway for further upregulation of Bcl2 and

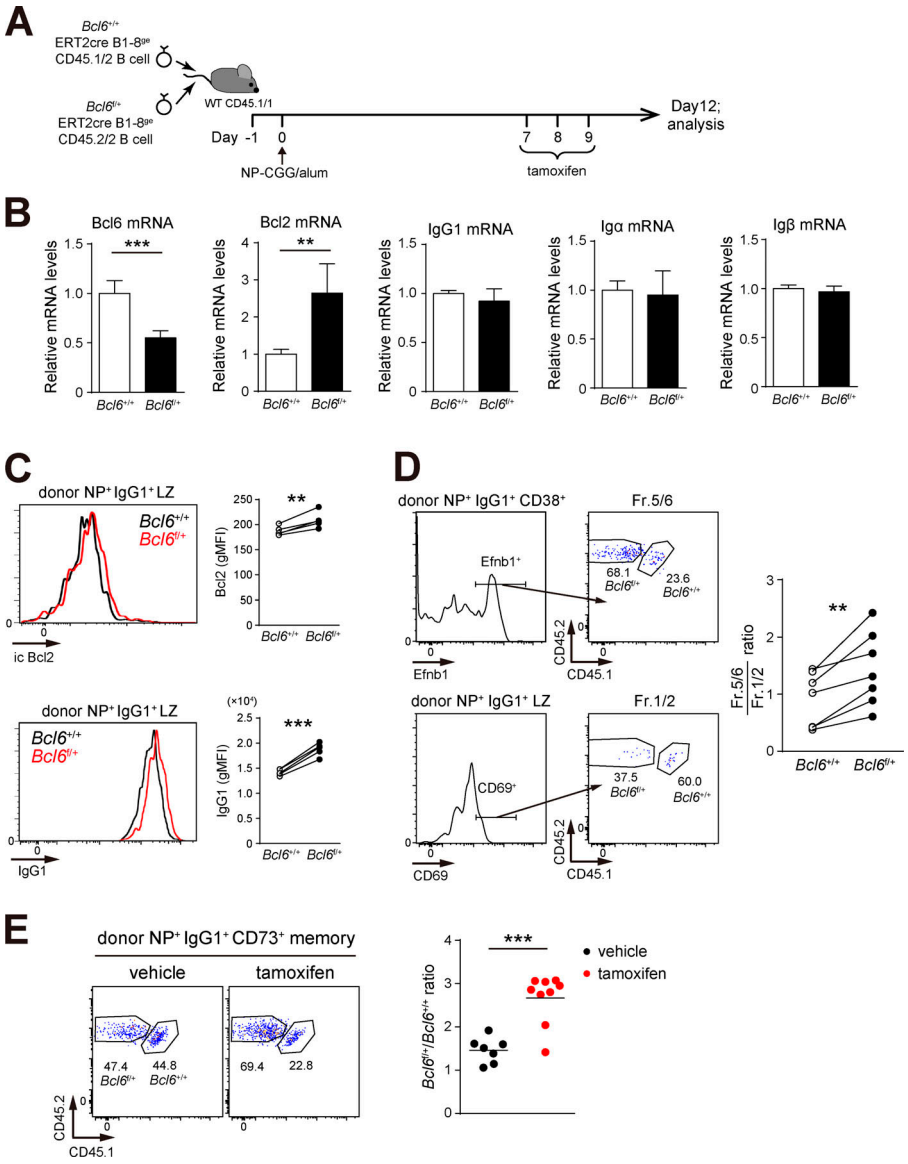

Figure 7. **Increased Bcl2 and BCR expression in GC B cells induced by Bcl6 haploinsufficiency. (A)** Experimental protocol for the assessment of the effect of inducible Bcl6 haploinsufficiency in GC B cells on memory B cell generation. Congenically marked *Bcl6*$^{+/+}$ and *Bcl6*$^{f/+}$ ERT2cre B1-8^{ge} naive B cells were cotransferred as a 1:1 mixture into wild-type CD45.1/1 mice, which were immunized with NP-CGG/alum, administered with tamoxifen on days 7–9, and analyzed on day 12. **(B)** Relative mRNA expression of Bcl6, Bcl2, IgG1, Igα, and Igβ genes in LZ B cells determined by real-time qPCR analysis. *n* = 4 (Bcl6, IgG1, Igα, Igβ), *n* = 5 (Bcl2), pooled from two independent experiments. **(C)** Left: Flow cytometry analysis of intracellular (ic) Bcl2 and surface IgG1 expression in donor NP$^+$IgG1$^+$LZ B cells. Right: Cumulative data of geometric mean fluorescence intensity (gMFI). *n* = 5, pooled from two independent experiments. **(D)** Left: Flow cytometry analysis of donor NP$^+$IgG1$^+$CD38$^+$ and NP$^+$IgG1$^+$LZ B cells. Right: Cumulative data of Fr.5/6 to Fr.1/2 ratio. *n* = 7, pooled from two independent experiments. **(E)** Left: Flow cytometry analysis of donor NP$^+$IgG1$^+$CD73$^+$ memory B cells. Right: Cumulative data of *Bcl6*$^{f/+}$:*Bcl6*$^{+/+}$ ratio. *n* = 7 (vehicle), *n* = 9 (tamoxifen), pooled from two independent experiments. **, P < 0.01; ***, P < 0.001; unpaired Student's *t* test (B and E) and **, P < 0.01; ***, P < 0.001; paired Student's *t* test (C and D).

surface BCR during differentiation toward mature memory B cells. In regard to this differentiation pathway, our data using Bcl6 haploinsufficiency are highly complementary to previous in vitro data that ectopic expression of Bcl6 in B cell cultures blocks the GC B cells from differentiating into memory B cells (Kuo et al., 2007). Together, it is likely that stepwise decreases in Bcl6 expression (pro-memory > pre-memory > mature memory B cells) play a key role in memory B cell development. This raises the question of how is Bcl6 downregulated. Three possibilities have already been reported: (1) upon strong BCR engagement, Erk-mediated degradation of Bcl6 (Niu et al., 1998); (2) transcriptional downregulation of Bcl6, mediated by CD40-activated IRF4 (Saito et al., 2007); and (3) downregulation of Bcl6 by defective IL-21 signaling (Linterman et al., 2010). Among these, in regard to differentiation from GC to memory B cells, the final possibility seems to best fit with our observation that pro-memory B cells possess lower-affinity BCRs, thereby receiving less T cell help. In addition, as a transcriptional circuit–type regulation, the transcription factor Hhex, critical for memory B cell differentiation, has been recently reported to participate in downregulation of Bcl6 (Laidlaw et al., 2020).

In summary, this study provides important insights into the initial events for the fate decisions from GC to memory B cells; the modulation of cellular metabolism and survival play fundamental roles. Given the importance of GC-derived memory B cells for protection against heterologous virus reinfection (Leach et al., 2019; Purtha et al., 2011), our findings may contribute to the development of efficient vaccination strategies.

Materials and methods

Mice

Bach2$^{f/f}$ (Kometani et al., 2013), Bcl6-YFP (Kitano et al., 2011), mVenus-p27K$^-$ transgenic (Oki et al., 2014), B1-8^{hi} (Shih et al., 2002), B1-8^{ge} (Shinnakasu et al., 2016), B1-8^{ge}-flox (Kometani et al., 2013), *Mtor*^{F2108L} (Ersching et al., 2017), and *Bcl6*$^{f/f}$ mice (Ise et al., 2014) were described previously. *Prdm1*$^{f/f}$ mice were purchased from Jackson Laboratory (JAX #008100). *Rosa26*-

ERT2cre mice were purchased from Taconic Biosciences. C57BL/6 mice were purchased from CLEA Japan. Bim-flox mice were generated by homologous recombination using Bruce 4 embryonic stem cells so that the exon encoding the BH3 domain of the *Bcl2l11* gene was flanked with two loxP sites. Chimeric mice were produced by microinjection of positive embryonic stem clones and then crossed with C57BL/6 mice to obtain germline-transmitted animals. Sex-matched 7–15-wk-old mice were used for all animal experiments. Mice were bred and maintained under specific pathogen–free conditions, and all animal experiments were performed under the institutional guidelines of Osaka University.

Immunization, adoptive transfer, and treatments

Mice were immunized by i.p. injection with 30 µg NP conjugated to CGG precipitated with 10% aluminum sulfate (Wako). Adoptive transfer experiments were performed as described previously (Shinnakasu et al., 2016). In brief, splenic B cells were purified by magnetic cell depletion using anti-CD43 microbeads and the AutoMACS system (Miltenyi Biotec). Purified B1-8 B cells containing 0.5–1 × 10^5 NP-binders (a 1:1 mixture of 2.5–5 × 10^4 NP-binders for cotransfer experiments) were transferred i.v. into recipient mice. Deletion of the loxP-flanked alleles in *Rosa26*-ERT2cre mice was induced by oral administration of 2 or 3 mg tamoxifen (Sigma-Aldrich) in sunflower oil once per day for 1–3 d. Rapamycin (Tokyo Chemical Industry) was injected i.p. at 0.16 mg/kg in 200 µl of 5% PEG 400 (Sigma-Aldrich)/5% Tween 80 (Sigma-Aldrich) once per day at the indicated time points. EdU (1 mg/200 µl in PBS; Thermo Fisher Scientific) was injected i.p., and the mice were further treated with 0.4 mg/ml EdU in the drinking water for 3 d when necessary.

Flow cytometry and cell sorting

Single-cell suspensions of splenocytes were analyzed and sorted on a FACSCanto II (BD Biosciences) or a FACSAria II (BD Biosciences). Alexa647-active caspase-3, V500-B220, V450-Bcl6, BV786-CD138, BV510-CD38, V500-CD45.2, BV510-IgG1, PE-IgG1 antibodies, and BV786-streptavidin were purchased from BD Biosciences. APC-eFluor780-B220, FITC-CD45.1, PE-CD45.1, APC-eFluor780-CD45.1, FITC-CD45.2, APC-eFluor780-CD45.2, APC-CD69, APC-eFluor780-CD69, eFluor450-CD73, PE-CD86, PerCP-Cy5.5-GL7 antibodies, PerCP-Cy5.5-streptavidin, PE-streptavidin, and APC-eFluor780-streptavidin were purchased from eBioscience. PE-B220, PE-Cy7-CD138, PE-Cy7-CD38, PacificBlue-CD45.1, PE-CD45.2, biotin-CD69, PerCP-Cy5.5-CD86, BV421-CXCR4, V450-Ki67 antibodies, and BV510-streptavidin were purchased from BioLegend. PE-pRb and PE-pS6 antibodies were purchased from Cell Signaling. c-Myc antibody was purchased from Abcam. PE-Bcl2 antibody was purchased from Miltenyi Biotec. Biotin-Efnb1 antibody was purchased from R&D Systems. Alexa488-goat anti-rabbit IgG antibody was purchased from Thermo Fisher Scientific. For intracellular staining, the cells were fixed and permeabilized using a Foxp3 staining kit (eBioscience) for Bcl6, Bcl2, and pRb, a BD Cytofix/Cytoperm solution (BD Biosciences) for pS6 and active caspase-3, or a True-Nuclear Transcription Factor Staining Buffer Set (BioLegend) for c-Myc. APC-conjugated NP was prepared as described previously (Shinnakasu et al., 2016). Incorporation of EdU was detected using a Click-iT Plus EdU Flow Cytometry Assay Kit (Thermo Fisher Scientific) according to the manufacturer's instructions.

Recall assay for GC and memory B cells

The recall potential of GC LZ B cell subsets and memory B cells was assessed as follows. In Fig. 1, F and G, Bcl6-YFP B1-8^{hi} $CD45.1^+$ naive B cells were transferred to C57BL/6 wild-type mice and immunized with NP-CGG/alum. 10–12 d later, NP-specific $IgG1^+$ donor Fr.2, Fr.3, Fr.5, and Fr.6 cells were sorted from splenocytes of 10 mice per experiment after enrichment of donor B cells by magnetic cell sorting depletion using biotin-CD45.2 antibody and streptavidin microbeads (Miltenyi Biotec). In Fig. 5 F, B1-8^{ge} $CD45.1^+$ naive B cells were transferred to $Mtor^{F2108L}$ mice and immunized with NP-CGG/alum (day 0), followed by rapamycin administration on days 4–12. On day 14, NP-specific $IgG1^+$ donor memory B cells ($Dump^-CD45.1^+NP^+IgG1^+CD38^+$) were sorted from splenocytes of five mice per experiment after enrichment of donor B cells by magnetic cell sorting depletion using biotinylated antibodies (IgM, IgD, F4/80, Gr-1, Ter119, NK1.1, Thy1.2, and CD5) and streptavidin microbeads. Sorted B cells (2 × 10^4 per recipient for Fig. 1, F and G; 2 × 10^3 per recipient for Fig. 5 F) were transferred i.v. together with activated $CD4^+$ T cells (10^7 per recipient) from CGG-immunized mice into sublethally irradiated (4.0 Gy) wild-type mice. Mice were then rechallenged with NP-CGG (50 µg) immunization i.p. on the next day (day 0) and analyzed on day 6.

RNA-seq and data analysis

RNA-seq data used in Fig. 1, C and D; Fig. 2, A, D, and E; Fig. 6, B and D; Fig. S1 D; Fig. S2 A; Fig. S3; and Fig. S4 are derived from two or three biological replicates. Bcl6-YFP B1-8^{hi} naive B cells were transferred into wild-type $CD45.1^+$ mice. Mice were immunized i.p. (day 0) with NP-CGG/alum and NP-specific $IgG1^+$ donor ([LZ; $CD45.2^+NP^+CD138^-IgG1^+CD38^-CD86^{hi}CXCR4^{lo}$], [Fr.2; $CD45.2^+NP^+CD138^-IgG1^+CD38^-CD86^{hi}CXCR4^{lo}$Bcl6-$YFP^{hi}CD69^{hi}$], [Fr.3; $CD45.2^+NP^+CD138^-IgG1^+CD38^-CD86^{hi}CXCR4^{lo}$Bcl6-$YFP^{hi}$ $CD69^{lo}$], [Fr.5; $CD45.2^+NP^+CD138^-IgG1^+CD38^+GL7^-$Bcl6-$YFP^{hi}$ $Efnb1^{hi}$], [Fr.6; $CD45.2^+NP^+CD138^-IgG1^+CD38^+GL7^-$Bcl6-$YFP^{lo}$ $Efnb1^{hi}$], and [Fr.7; $CD45.2^+NP^+CD138^-IgG1^+CD38^+GL7^-$Bcl6-$YFP^{lo}Efnb1^{lo}$]) B cells were sorted from pooled splenocytes of nine recipient mice on day 10. RNA-seq data used in Fig. 3 C and Fig. S2 B are derived from two biological replicates. *Bach2*$^{+/+}$*Prdm1*$^{f/f}$ ERT2cre B1-8^{hi} or *Bach2*$^{f/f}$*Prdm1*$^{f/f}$ ERT2cre B1-8^{hi} naive B cells were transferred independently into wild-type CD45.1/45.2 mice. After administration of tamoxifen (3 mg) for 3 d, mice were immunized i.p. (day 0) with NP-CGG/alum, and NP-specific donor GC DZ ($CD45.1^-CD45.2^+NP^+GL7^+CD38^-CD86^{lo}CXCR4^{hi}$) and LZ ($CD45.1^-CD45.2^+NP^+GL7^+CD38^-CD86^{hi}CXCR4^{lo}$) B cells were sorted from pooled splenocytes of five recipient mice on day 10.

Construction of the DNA library for RNA-seq and sequencing were performed as described previously (Shinnakasu et al., 2016). Briefly, the DNA library was constructed using the NEBNext Ultra RNA Library Prep Kit for Illumina (New England Biolabs) from total RNA purified from ∼10^4 sorted cells. RNA-seq was performed on a HiSeq 1500 sequencer (Illumina) in a

49-bp single-end read mode. The raw data were processed with CASAVA 1.8.2 (Illumina) to generate fastq files. The RNA-seq data were deposited in the Gene Expression Omnibus database under accession nos. GSE146922 and GSE147095. GSEA was performed with GSEA software from the Broad Institute (Subramanian et al., 2005).

BCR cloning and antibody expression

NP-specific IgG1$^+$ Fr.2 (B220$^+$NP$^+$CD138$^-$IgG1$^+$CD38$^-$CD86^{hi} CXCR4^{lo}Bcl6-YFP^{hi}CD69^{hi}) and Fr.5 (B220$^+$NP$^+$CD138$^-$IgG1$^+$CD38$^+$ GL7$^-$Bcl6-YFP^{hi}Efnb1^{hi}) B cells were single-cell sorted from a spleen of single Bcl6-YFP mouse 11 d after i.p. immunization with NP-CGG/alum. Cloning and expression of NP-specific antibodies were performed as described previously (von Boehmer et al., 2016) with the following modifications. PCR-amplified Igγ1 and Igλ V(D)J transcripts were cloned into the human Igγ1/Igλ-expression vector (pVITRO1-dV-IgG1/λ; Dodev et al., 2014; Addgene #52214) using the seamless ligation cloning extract (SLiCE) method (Motohashi, 2015). The heavy and light chain pairing of the IGHV1-72*01 and IGLV1*01 genes was confirmed by IMGT/V-QUEST analysis (http://www.imgt.org; Brochet et al., 2008). Monoclonal antibodies were expressed using the Expi293 Expression System (Thermo Fisher Scientific) and purified from the culture supernatants of Expi293F cells by Protein G Sepharose (GE).

ELISA

The 96-well plates (Nunc MaxiSorp, Thermo Fisher Scientific) were coated with 2 µg/ml of NP_{29}-BSA or NP_1-BSA for the capture of antibodies. After blocking with BlockingOne reagent (Nacalai), the plates were incubated with serially diluted monoclonal antibodies, starting at 1 µg/ml. NP-specific IgG1 antibodies were detected using horseradish peroxidase–conjugated goat anti-human IgG (Southern Biotech) with SureBlue TMB substrate (KPL). The absorbance at 450 nm was measured with a microplate reader (ARVO X3, PerkinElmer). Fig. 2 B represents the measurements at 0.33 µg/ml antibody concentration.

Real-time quantitative PCR (qPCR) analysis

Real-time qPCR was performed as described previously (Inoue et al., 2015). *Actb* mRNA levels were used for normalization. The following primers were used for qPCR analysis: IgG1-forward, 5′-TGCACAACCACCATACTGAGA-3′; IgG1-reverse, 5′-ATGGTG ATGGTCGTCCAGAG-3′; *Bcl6*-forward, 5′-GCAGACGCACAGTGA CAAACC-3′; *Bcl6*-reverse, 5′-GAATTCGAGTGTGGGTCTTCAGG-3′; *Bcl2*-forward, 5′-ATGACTGAGTACCTGAACCGGC-3′; *Bcl2*-reverse, 5′-AAACAGAGGTCGCATGCTGG-3′; *Cd79a*-forward, 5′-ACCGCATCATCACAGCAGAAGG-3′; *Cd79a*-reverse, 5′-TCC TGGTAGGTGCCCTGGA-3′; *Cd79b*-forward, 5′-GCTGTTGTT CCTGCTGCTGC-3′; *Cd79b*-reverse, 5′-CTTCACCATGGAGCT CCGCTTT-3′; *Bcl2l11*-forward, 5′-CGACAGTCTCAGGAGGAA CC-3′; *Bcl2l11*-reverse, 5′-CCTTCTCCATACCAGACGGA-3′; *Actb* forward, 5′-CCGCCACCAGTTCGCCATG-3′; and *Actb* reverse, 5′-TACAGCCCGGGGAGCATCGT-3′.

Statistical analysis

Statistical analyses were performed by a two-tailed unpaired and paired Student's *t* test using GraphPad Prism software. P values <0.05 were considered significant (*, P < 0.05; **, P < 0.01; ***, P < 0.001). Error bars denote ± SD.

Online supplemental material

Fig. S1 shows full gating strategy of Fig. 1 A data, cell number kinetics of Fr.2, 3, 5, 6, and 7 cells in spleen 8, 10, 12, 14, and 20 d after immunization of wild-type mice, gating strategy for RNA-seq analysis (related to Fig. 1, C and D), comparison of *S1pr2* and *Gpr183* gene expression between Fr.6 and LZ B cells, and comparison of Ki67 protein expression between Fr.5 and preGC B cells. Fig. S2 shows heatmap analysis of the top 50 most differentially expressed genes in RNA-seq data. Fig. S3 shows comparison of *Bach2*, *Bcl6*, *Ccr6*, and *Efnb1* gene expression among memory precursor populations. Fig. S4 shows comparison of gene expression profiles and pS6, c-Myc, and pRb protein expression between Fr.2 and Fr.5 cells. Fig. S5 shows comparison of pS6 and c-Myc protein expression between Fr.3 and Fr.5 cells, frequency of *Bcl2l11*$^{f/+}$ NP$^+$IgG1$^+$CD73$^+$ memory B cells (related to Fig. 6 E), frequency of apoptotic cells among total LZ GC cells upon BCR downregulation (related to Fig. 6 H), and evaluation of nonspecific effect on apoptosis induced by Cre-mediated double-strand breaks (related to Fig. 6 H).

Acknowledgments

We thank M.C. Nussenzweig (The Rockefeller University, New York, NY) for B1-8^{hi} mice, T. Okada (RIKEN Center for Integrative Medical Sciences, Kanagawa, Japan) for Bcl6-YFP mice, G.D. Victora (The Rockefeller University) for *Mtor*^{F2108L} mice, and P.D. Burrows for critical reading of the manuscript.

This work was supported by grants from JSPS KAKENHI (JP17K08882 to T. Inoue; JP26221306 and JP19H01028 to T. Kurosaki), the SENSHIN Medical Research Foundation (to T. Inoue), the Mochida Memorial Foundation for Medical and Pharmaceutical Research (to T. Inoue), and a research grant from Astellas Foundation for Research on Metabolic Disorders (to T. Inoue).

Author contributions: T. Inoue and C. Kawai performed the experiments; T. Inoue and T. Kurosaki designed the experiments; R. Shinnakasu, W. Ise, T. Oki, T. Kitamura, and H. Fukuyama provided essential reagents; E. Kawakami, N. Sax, and K. Yamashita performed bioinformatics analyses; T. Inoue and T. Kurosaki wrote the manuscript.

Disclosures: The authors declare no competing interests exist.

Submitted: 1 May 2020
Revised: 11 August 2020
Accepted: 3 September 2020

References

Allen, C.D., T. Okada, H.L. Tang, and J.G. Cyster. 2007. Imaging of germinal center selection events during affinity maturation. *Science*. 315:528–531. https://doi.org/10.1126/science.1136736

Bannard, O., R.M. Horton, C.D. Allen, J. An, T. Nagasawa, and J.G. Cyster. 2013. Germinal center centroblasts transition to a centrocyte phenotype according to a timed program and depend on the dark zone for effective

selection. *Immunity*. 39:912–924. https://doi.org/10.1016/j.immuni.2013.08.038

Boothby, M., and R.C. Rickert. 2017. Metabolic Regulation of the Immune Humoral Response. *Immunity*. 46:743–755. https://doi.org/10.1016/j.immuni.2017.04.009

Brochet, X., M.P. Lefranc, and V. Giudicelli. 2008. IMGT/V-QUEST: the highly customized and integrated system for IG and TR standardized V-J and V-D-J sequence analysis. *Nucleic Acids Res*. 36(Web Server issue, Web Server):W503–W508. https://doi.org/10.1093/nar/gkn316

Calado, D.P., Y. Sasaki, S.A. Godinho, A. Pellerin, K. Köchert, B.P. Sleckman, I.M. de Alborán, M. Janz, S. Rodig, and K. Rajewsky. 2012. The cell-cycle regulator c-Myc is essential for the formation and maintenance of germinal centers. *Nat. Immunol*. 13:1092–1100. https://doi.org/10.1038/ni.2418

Dodev, T.S., P. Karagiannis, A.E. Gilbert, D.H. Josephs, H. Bowen, L.K. James, H.J. Bax, R. Beavil, M.O. Pang, H.J. Gould, et al. 2014. A tool kit for rapid cloning and expression of recombinant antibodies. *Sci. Rep*. 4:5885. https://doi.org/10.1038/srep05885

Dominguez-Sola, D., G.D. Victora, C.Y. Ying, R.T. Phan, M. Saito, M.C. Nussenzweig, and R. Dalla-Favera. 2012. The proto-oncogene MYC is required for selection in the germinal center and cyclic reentry. *Nat. Immunol*. 13:1083–1091. https://doi.org/10.1038/ni.2428

Dominguez-Sola, D., J. Kung, A.B. Holmes, V.A. Wells, T. Mo, K. Basso, and R. Dalla-Favera. 2015. The FOXO1 Transcription Factor Instructs the Germinal Center Dark Zone Program. *Immunity*. 43:1064–1074. https://doi.org/10.1016/j.immuni.2015.10.015

Ersching, J., A. Efeyan, L. Mesin, J.T. Jacobsen, G. Pasqual, B.C. Grabiner, D. Dominguez-Sola, D.M. Sabatini, and G.D. Victora. 2017. Germinal Center Selection and Affinity Maturation Require Dynamic Regulation of mTORC1 Kinase. *Immunity*. 46:1045–1058.e6. https://doi.org/10.1016/j.immuni.2017.06.005

Finkin, S., H. Hartweger, T.Y. Oliveira, E.E. Kara, and M.C. Nussenzweig. 2019. Protein Amounts of the MYC Transcription Factor Determine Germinal Center B Cell Division Capacity. *Immunity*. 51:324–336.e5. https://doi.org/10.1016/j.immuni.2019.06.013

Fischer, S.F., P. Bouillet, K. O'Donnell, A. Light, D.M. Tarlinton, and A. Strasser. 2007. Proapoptotic BH3-only protein Bim is essential for developmentally programmed death of germinal center-derived memory B cells and antibody-forming cells. *Blood*. 110:3978–3984. https://doi.org/10.1182/blood-2007-05-091306

Grant, F.M., J. Yang, R. Nasrallah, J. Clarke, F. Sadiyah, S.K. Whiteside, C.J. Imianowski, P. Kuo, P. Vardaka, T. Todorov, et al. 2020. BACH2 drives quiescence and maintenance of resting Treg cells to promote homeostasis and cancer immunosuppression. *J. Exp. Med*. 217. e20190711. https://doi.org/10.1084/jem.20190711

Igarashi, K., T. Kurosaki, and R. Roychoudhuri. 2017. BACH transcription factors in innate and adaptive immunity. *Nat. Rev. Immunol*. 17:437–450. https://doi.org/10.1038/nri.2017.26

Inoue, T., M. Morita, A. Hijikata, Y. Fukuda-Yuzawa, S. Adachi, K. Isono, T. Ikawa, H. Kawamoto, H. Koseki, T. Natsume, et al. 2015. CNOT3 contributes to early B cell development by controlling Igh rearrangement and p53 mRNA stability. *J. Exp. Med*. 212:1465–1479. https://doi.org/10.1084/jem.20150384

Inoue, T., R. Shinnakasu, W. Ise, C. Kawai, T. Egawa, and T. Kurosaki. 2017. The transcription factor Foxo1 controls germinal center B cell proliferation in response to T cell help. *J. Exp. Med*. 214:1181–1198. https://doi.org/10.1084/jem.20161263

Inoue, T., I. Moran, R. Shinnakasu, T.G. Phan, and T. Kurosaki. 2018. Generation of memory B cells and their reactivation. *Immunol. Rev*. 283:138–149. https://doi.org/10.1111/imr.12640

Ise, W., T. Inoue, J.B. McLachlan, K. Kometani, M. Kubo, T. Okada, and T. Kurosaki. 2014. Memory B cells contribute to rapid Bcl6 expression by memory follicular helper T cells. *Proc. Natl. Acad. Sci. USA*. 111:11792–11797. https://doi.org/10.1073/pnas.1404671111

Ise, W., K. Fujii, K. Shiroguchi, A. Ito, K. Kometani, K. Takeda, E. Kawakami, K. Yamashita, K. Suzuki, T. Okada, et al. 2018. T Follicular Helper Cell-Germinal Center B Cell Interaction Strength Regulates Entry into Plasma Cell or Recycling Germinal Center Cell Fate. *Immunity*. 48:702–715.e4. https://doi.org/10.1016/j.immuni.2018.03.027

Kitano, M., S. Moriyama, Y. Ando, M. Hikida, Y. Mori, T. Kurosaki, and T. Okada. 2011. Bcl6 protein expression shapes pre-germinal center B cell dynamics and follicular helper T cell heterogeneity. *Immunity*. 34:961–972. https://doi.org/10.1016/j.immuni.2011.03.025

Kometani, K., R. Nakagawa, R. Shinnakasu, T. Kaji, A. Rybouchkin, S. Moriyama, K. Furukawa, H. Koseki, T. Takemori, and T. Kurosaki. 2013. Repression of the transcription factor Bach2 contributes to predisposition of IgG1 memory B cells toward plasma cell differentiation. *Immunity*. 39:136–147. https://doi.org/10.1016/j.immuni.2013.06.011

Kuo, T.C., A.L. Shaffer, J. Haddad, Jr., Y.S. Choi, L.M. Staudt, and K. Calame. 2007. Repression of BCL-6 is required for the formation of human memory B cells in vitro. *J. Exp. Med*. 204:819–830. https://doi.org/10.1084/jem.20062104

Laidlaw, B.J., T.H. Schmidt, J.A. Green, C.D. Allen, T. Okada, and J.G. Cyster. 2017. The Eph-related tyrosine kinase ligand Ephrin-B1 marks germinal center and memory precursor B cells. *J. Exp. Med*. 214:639–649. https://doi.org/10.1084/jem.20161461

Laidlaw, B.J., L. Duan, Y. Xu, S.E. Vazquez, and J.G. Cyster. 2020. The transcription factor Hhex cooperates with the corepressor Tle3 to promote memory B cell development. *Nat. Immunol*. 21:1082–1093. https://doi.org/10.1038/s41590-020-0713-6

Lam, K.P., R. Kühn, and K. Rajewsky. 1997. In vivo ablation of surface immunoglobulin on mature B cells by inducible gene targeting results in rapid cell death. *Cell*. 90:1073–1083. https://doi.org/10.1016/S0092-8674(00)80373-6

Leach, S., R. Shinnakasu, Y. Adachi, M. Momota, C. Makino-Okamura, T. Yamamoto, K.J. Ishii, H. Fukuyama, Y. Takahashi, and T. Kurosaki. 2019. Requirement for memory B-cell activation in protection from heterologous influenza virus reinfection. *Int. Immunol*. 31:771–779. https://doi.org/10.1093/intimm/dxz049

Liberzon, A., C. Birger, H. Thorvaldsdóttir, M. Ghandi, J.P. Mesirov, and P. Tamayo. 2015. The Molecular Signatures Database (MSigDB) hallmark gene set collection. *Cell Syst*. 1:417–425. https://doi.org/10.1016/j.cels.2015.12.004

Linterman, M.A., L. Beaton, D. Yu, R.R. Ramiscal, M. Srivastava, J.J. Hogan, N.K. Verma, M.J. Smyth, R.J. Rigby, and C.G. Vinuesa. 2010. IL-21 acts directly on B cells to regulate Bcl-6 expression and germinal center responses. *J. Exp. Med*. 207:353–363. https://doi.org/10.1084/jem.20091738

Lu, P., C. Shih, and H. Qi. 2017. Ephrin B1-mediated repulsion and signaling control germinal center T cell territoriality and function. *Science*. 356. eaai9264. https://doi.org/10.1126/science.aai9264

Mayer, C.T., A. Gazumyan, E.E. Kara, A.D. Gitlin, J. Golijanin, C. Viant, J. Pai, T.Y. Oliveira, Q. Wang, A. Escolano, et al. 2017. The microanatomic segregation of selection by apoptosis in the germinal center. *Science*. 358. eaao2602. https://doi.org/10.1126/science.aao2602

Motohashi, K. 2015. A simple and efficient seamless DNA cloning method using SLiCE from Escherichia coli laboratory strains and its application to SLiP site-directed mutagenesis. *BMC Biotechnol*. 15:47. https://doi.org/10.1186/s12896-015-0162-8

Niu, H., B.H. Ye, and R. Dalla-Favera. 1998. Antigen receptor signaling induces MAP kinase-mediated phosphorylation and degradation of the BCL-6 transcription factor. *Genes Dev*. 12:1953–1961. https://doi.org/10.1101/gad.12.13.1953

O'Connor, L., A. Strasser, L.A. O'Reilly, G. Hausmann, J.M. Adams, S. Cory, and D.C. Huang. 1998. Bim: a novel member of the Bcl-2 family that promotes apoptosis. *EMBO J*. 17:384–395. https://doi.org/10.1093/emboj/17.2.384

O'Sullivan, T.E., L.R. Johnson, H.H. Kang, and J.C. Sun. 2015. BNIP3- and BNIP3L-Mediated Mitophagy Promotes the Generation of Natural Killer Cell Memory. *Immunity*. 43:331–342. https://doi.org/10.1016/j.immuni.2015.07.012

Oki, T., K. Nishimura, J. Kitaura, K. Togami, A. Maehara, K. Izawa, A. Sakaue-Sawano, A. Niida, S. Miyano, H. Aburatani, et al. 2014. A novel cell-cycle-indicator, mVenus-p27K-, identifies quiescent cells and visualizes G0-G1 transition. *Sci. Rep*. 4:4012. https://doi.org/10.1038/srep04012

Purtha, W.E., T.F. Tedder, S. Johnson, D. Bhattacharya, and M.S. Diamond. 2011. Memory B cells, but not long-lived plasma cells, possess antigen specificities for viral escape mutants. *J. Exp. Med*. 208:2599–2606. https://doi.org/10.1084/jem.20110740

Ridderstad, A., and D.M. Tarlinton. 1998. Kinetics of establishing the memory B cell population as revealed by CD38 expression. *J. Immunol*. 160:4688–4695.

Saito, M., J. Gao, K. Basso, Y. Kitagawa, P.M. Smith, G. Bhagat, A. Pernis, L. Pasqualucci, and R. Dalla-Favera. 2007. A signaling pathway mediating downregulation of BCL6 in germinal center B cells is blocked by BCL6 gene alterations in B cell lymphoma. *Cancer Cell*. 12:280–292. https://doi.org/10.1016/j.ccr.2007.08.011

Saito, M., U. Novak, E. Piovan, K. Basso, P. Sumazin, C. Schneider, M. Crespo, Q. Shen, G. Bhagat, A. Califano, et al. 2009. BCL6 suppression of BCL2 via Miz1 and its disruption in diffuse large B cell lymphoma. *Proc.*

Natl. Acad. Sci. USA. 106:11294–11299. https://doi.org/10.1073/pnas.0903854106

Sander, S., V.T. Chu, T. Yasuda, A. Franklin, R. Graf, D.P. Calado, S. Li, K. Imami, M. Selbach, M. Di Virgilio, et al. 2015. PI3 Kinase and FOXO1 Transcription Factor Activity Differentially Control B Cells in the Germinal Center Light and Dark Zones. *Immunity*. 43:1075–1086. https://doi.org/10.1016/j.immuni.2015.10.021

Shih, T.A., M. Roederer, and M.C. Nussenzweig. 2002. Role of antigen receptor affinity in T cell-independent antibody responses in vivo. *Nat. Immunol.* 3:399–406. https://doi.org/10.1038/ni776

Shinnakasu, R., T. Inoue, K. Kometani, S. Moriyama, Y. Adachi, M. Nakayama, Y. Takahashi, H. Fukuyama, T. Okada, and T. Kurosaki. 2016. Regulated selection of germinal-center cells into the memory B cell compartment. *Nat. Immunol*. 17:861–869. https://doi.org/10.1038/ni.3460

Sidwell, T., Y. Liao, A.L. Garnham, A. Vasanthakumar, R. Gloury, J. Blume, P.P. Teh, D. Chisanga, C. Thelemann, F. de Labastida Rivera, et al. 2020. Attenuation of TCR-induced transcription by Bach2 controls regulatory T cell differentiation and homeostasis. *Nat. Commun*. 11:252. https://doi.org/10.1038/s41467-019-14112-2

Smith, K.G., U. Weiss, K. Rajewsky, G.J. Nossal, and D.M. Tarlinton. 1994. Bcl-2 increases memory B cell recruitment but does not perturb selection in germinal centers. *Immunity*. 1:803–813. https://doi.org/10.1016/S1074-7613(94)80022-7

Srinivasan, L., Y. Sasaki, D.P. Calado, B. Zhang, J.H. Paik, R.A. DePinho, J.L. Kutok, J.F. Kearney, K.L. Otipoby, and K. Rajewsky. 2009. PI3 kinase signals BCR-dependent mature B cell survival. *Cell*. 139:573–586. https://doi.org/10.1016/j.cell.2009.08.041

Stewart, I., D. Radtke, B. Phillips, S.J. McGowan, and O. Bannard. 2018. Germinal Center B Cells Replace Their Antigen Receptors in Dark Zones and Fail Light Zone Entry when Immunoglobulin Gene Mutations are Damaging. *Immunity*. 49:477–489.e7. https://doi.org/10.1016/j.immuni.2018.08.025

Suan, D., N.J. Kräutler, J.L.V. Maag, D. Butt, K. Bourne, J.R. Hermes, D.T. Avery, C. Young, A. Statham, M. Elliott, et al. 2017. CCR6 Defines Memory B Cell Precursors in Mouse and Human Germinal Centers, Revealing Light-Zone Location and Predominant Low Antigen Affinity. *Immunity*. 47:1142–1153.e4. https://doi.org/10.1016/j.immuni.2017.11.022

Subramanian, A., P. Tamayo, V.K. Mootha, S. Mukherjee, B.L. Ebert, M.A. Gillette, A. Paulovich, S.L. Pomeroy, T.R. Golub, E.S. Lander, et al. 2005. Gene set enrichment analysis: a knowledge-based approach for interpreting genome-wide expression profiles. *Proc. Natl. Acad. Sci. USA*. 102:15545–15550. https://doi.org/10.1073/pnas.0506580102

Suzuki, A., T. Kaisho, M. Ohishi, M. Tsukio-Yamaguchi, T. Tsubata, P.A. Koni, T. Sasaki, T.W. Mak, and T. Nakano. 2003. Critical roles of Pten in B cell homeostasis and immunoglobulin class switch recombination. *J. Exp. Med*. 197:657–667. https://doi.org/10.1084/jem.20021101

Victora, G.D., and M.C. Nussenzweig. 2012. Germinal centers. *Annu. Rev. Immunol*. 30:429–457. https://doi.org/10.1146/annurev-immunol-020711-075032

Victora, G.D., T.A. Schwickert, D.R. Fooksman, A.O. Kamphorst, M. Meyer-Hermann, M.L. Dustin, and M.C. Nussenzweig. 2010. Germinal center dynamics revealed by multiphoton microscopy with a photoactivatable fluorescent reporter. *Cell*. 143:592–605. https://doi.org/10.1016/j.cell.2010.10.032

von Boehmer, L., C. Liu, S. Ackerman, A.D. Gitlin, Q. Wang, A. Gazumyan, and M.C. Nussenzweig. 2016. Sequencing and cloning of antigen-specific antibodies from mouse memory B cells. *Nat. Protoc*. 11:1908–1923. https://doi.org/10.1038/nprot.2016.102

Wang, Y., J. Shi, J. Yan, Z. Xiao, X. Hou, P. Lu, S. Hou, T. Mao, W. Liu, Y. Ma, et al. 2017. Germinal-center development of memory B cells driven by IL-9 from follicular helper T cells. *Nat. Immunol*. 18:921–930. https://doi.org/10.1038/ni.3788

JEM

Supplemental material

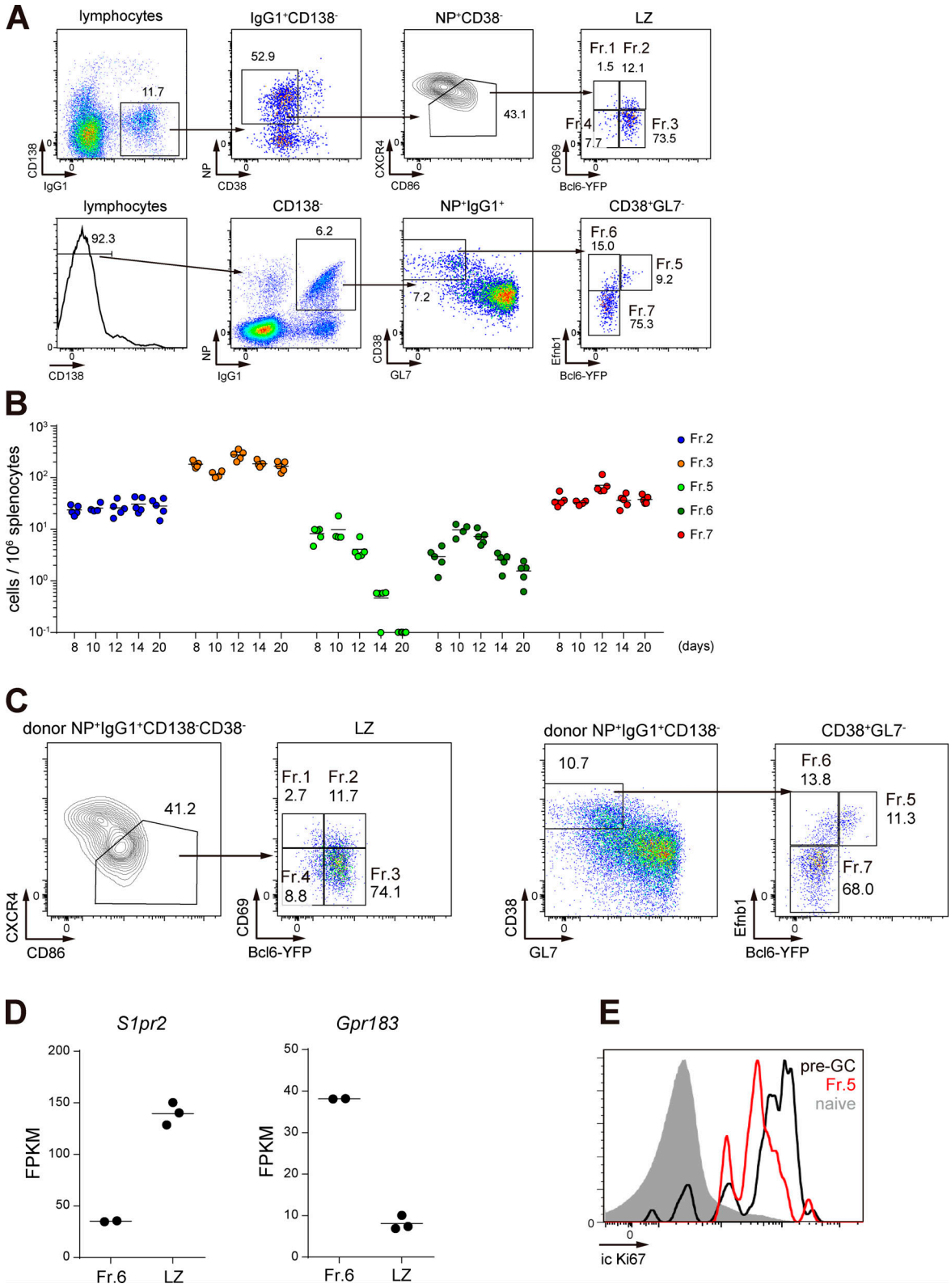

Figure S1. **Identification and characterization of pro-memory B cells (related to Fig. 1). (A)** Full gating strategy of Fig. 1 A data. **(B)** Cell number of NP$^+$ IgG1$^+$ Fr.2, Fr.3, Fr.5, Fr.6, and Fr.7 cells in spleen 8, 10, 12, 14, and 20 d after immunization of wild-type mice with NP-CGG/alum. n = 5 (day 8, 10, 12, 14), n = 4 (day 20), representative of two independent experiments. **(C)** Gating strategy of NP$^+$ IgG1$^+$ LZ, Fr.2, Fr.3, Fr.5, Fr.6, and Fr.7 cell sorting for RNA-seq analysis (described in Fig. 1, C and D). **(D)** *S1pr2* and *Gpr183* mRNA expression presented as fragments per kilobase of exon per million reads mapped (FPKM) values in RNA-seq data. Each dot represents a single RNA-seq sample. n = 2 (Fr.6), n = 3 (LZ). **(E)** Flow cytometry of intracellular (ic) Ki67 expression in naive B cells (B220$^+$CD38$^+$GL7$^-$) from unimmunized Bcl6-YFP mice, in preGC B cells (B220$^+$NP$^+$IgG1$^+$CD38$^+$GL7$^+$) from Bcl6-YFP mice 5 d after immunization, and in Fr.5 cells (B220$^+$NP$^+$IgG1$^+$CD38$^+$GL7$^-$Bcl6$^+$Efnb1$^+$) from Bcl6-YFP mice 10 d after immunization. Representative of three independent experiments.

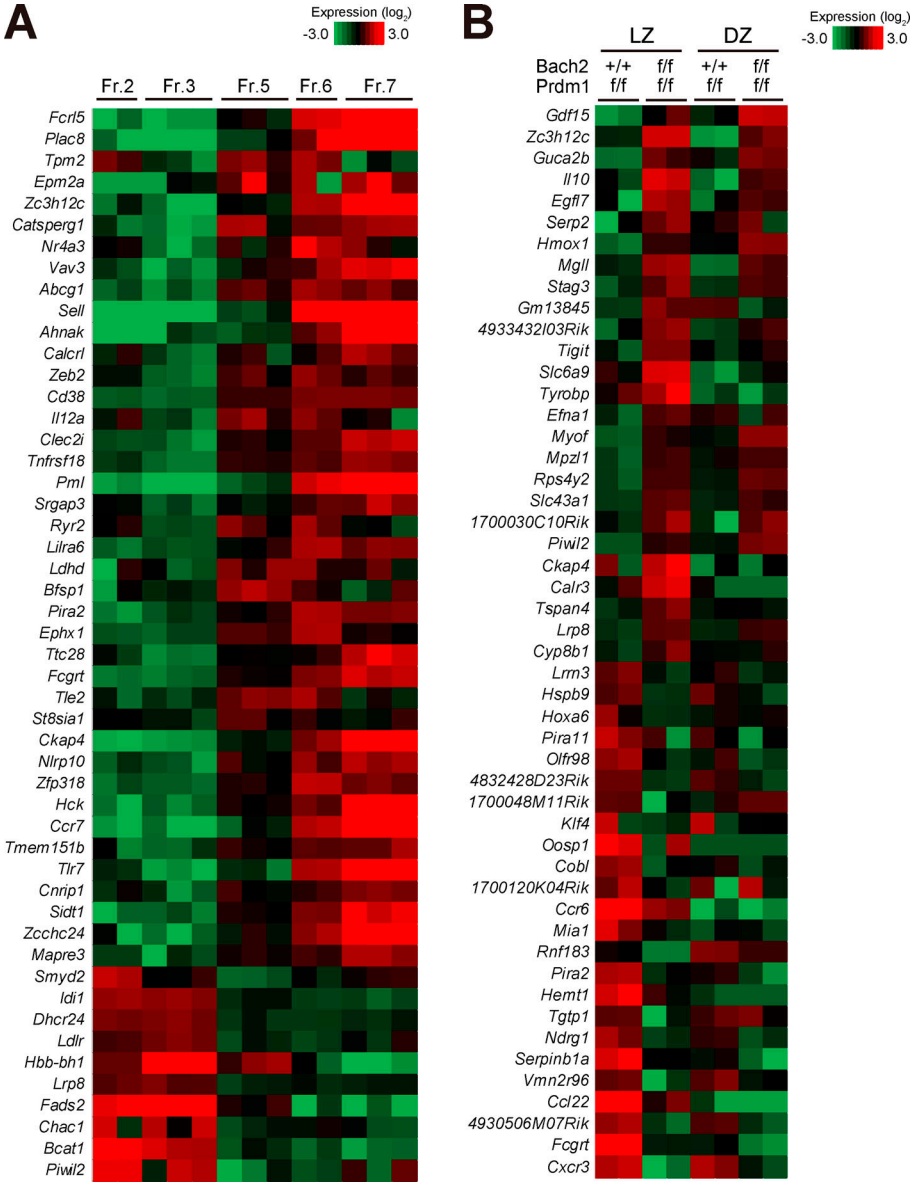

Figure S2. **Heatmap analysis of RNA-seq data. (A)** Heatmap illustrating the top 50 genes most differentially expressed between Fr.3 and Fr.5 cells (false discovery rate [FDR] P value < 0.05, $|\log_2$ fold change$|$ > 1.5). n = 2 (Fr.2, Fr.6), n = 3 (Fr.3, Fr.5, Fr.7). **(B)** Heatmap illustrating the top 50 genes most differentially expressed between *Bach2*$^{+/+}$*Prdm1*$^{f/f}$ LZ and *Bach2*$^{f/f}$*Prdm1*$^{f/f}$ LZ B cells (FDR P value < 0.05, $|\log_2$ fold change$|$ > 1.5). n = 2.

A

	Bach2	*Bcl6*	*Ccr6*	*Efnb1*	reference
Fr.5 (pro-memory)	hi	hi	int/lo	hi	GSE147095 (this study)
Fr.6 (pre-memory)	int	int/lo	hi/int	int	GSE147095 (this study)
Pop 4 (Efnb1^{+} S1pr2^{lo})	lo	lo	hi	lo	GSE89897 (Laidlaw et al., *J Exp Med*, 2017)
LZ CCR6^{+}	int	int	hi/int	N.A.	E-MTAB-3974 (Suan et al., *Immunity*, 2017)
mKO2^{hi}	int	int	hi	int	GSE85018 (Wang et al., *Nat Immunol*, 2017)

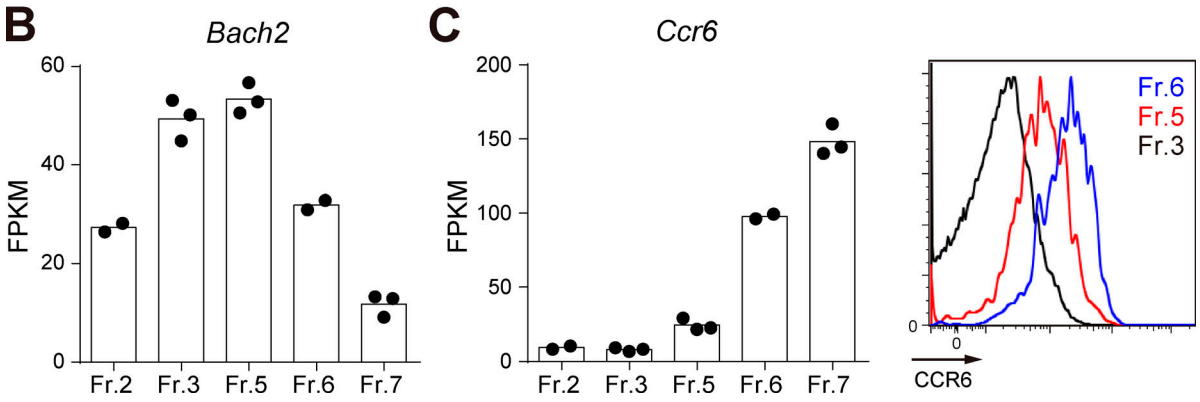

Figure S3. **Comparison of expression of selected genes among memory precursor populations. (A)** Comparison of mRNA expression of *Bach2*, *Bcl6*, *Ccr6*, and *Efnb1* genes in Fr.5 and Fr.6 cells with in previously reported memory precursor populations. hi, high; int, intermediate; lo, low; N.A., not available. **(B)** *Bach2* and (C, left) *Ccr6* mRNA expression presented as fragments per kilobase of exon per million reads mapped (FPKM) values in RNA-seq data (Fig. 1, C and D). Each dot represents single RNA-seq sample. *n* = 2 (Fr.2, Fr.6), *n* = 3 (Fr.3, Fr.5, Fr.7). **(C)** Right: Flow cytometry analysis of CCR6 expression in Fr.3, Fr.5, and Fr.6 cells. Representative of three independent experiments.

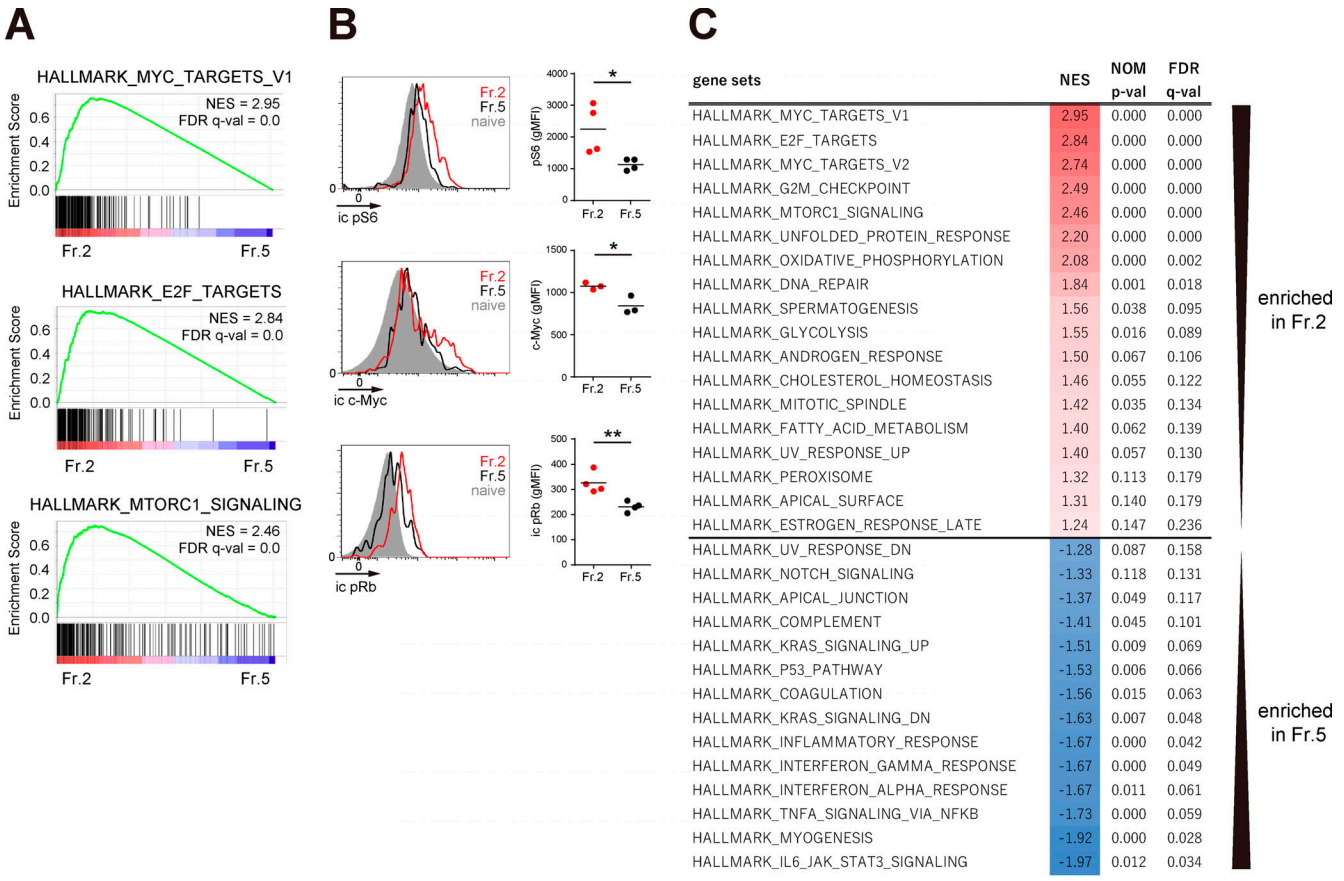

Figure S4. **Comparison of gene expression profile between Fr.2 and Fr.5 cells. (A)** GSEA of Fr.2 and Fr.5 RNA-seq data (Fig. 1, C and D). Selected gene sets are shown with normalized enrichment scores (NES) and false discovery rate (FDR) q-values (q-val). **(B)** Left: Flow cytometry analysis of intracellular (ic) expression of pS6, c-Myc, and pRb in Fr.2, Fr.5, and naive B cells. Right: Cumulative data of geometric mean fluorescence intensity (gMFI). $n = 4$ (pS6, pRb), $n = 3$ (c-Myc), representative of two independent experiments. **(C)** GSEA of Fr.2 and Fr.5 RNA-seq data. All Hallmark gene sets enriched in Fr.2 or Fr.5 (FDR q-value < 0.25) were listed with NES and nominal (NOM) P value (p-val). *, $P < 0.05$; **, $P < 0.01$; unpaired Student's t test.

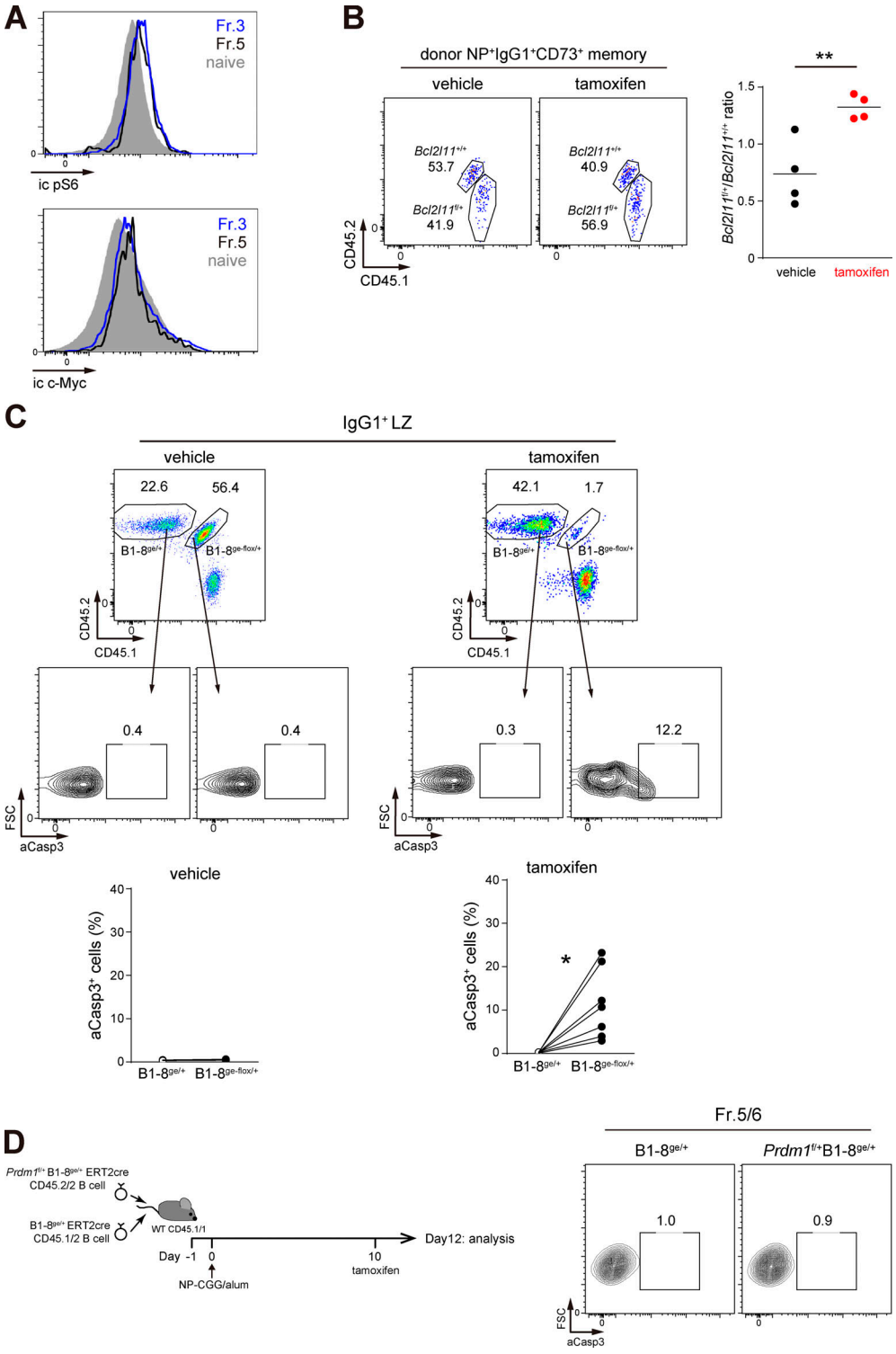

Figure S5. **Cellular survival of pro-memory B cells. (A)** Flow cytometry analysis of intracellular (ic) expression of pS6 and c-Myc in Fr. 3, Fr.5, and naive B cells (related to Fig. 2 C). Representative of three independent experiments. **(B)** Left: Flow cytometry analysis of donor NP$^+$IgG1$^+$CD73$^+$ memory B cells. Congenically marked *Bcl2l11*$^{+/+}$ and *Bcl2l11*$^{f/+}$ ERT2cre B1-8^{ge} naive B cells were cotransferred as a 1:1 mixture into wild-type mice, which were immunized with NP-CGG/alum, administered with tamoxifen on day 8, and analyzed on day 21 (see also Fig. 6 E). Right: Cumulative data of *Bcl2l11*$^{f/+}$:*Bcl2l11*$^{+/+}$ ratio. n = 4, representative of two independent experiments. **(C)** Top: Flow cytometry analysis of aCasp3 expression in donor IgG1$^+$ LZ B cells (related to Fig. 6, H and J). Bottom: Cumulative data of aCasp3$^+$ ratio. n = 4 (vehicle), n = 7 (tamoxifen), pooled from two independent experiments. **(D)** Left: Protocol of the control experiment related to Fig 6 H. Congenically marked B1-8^{ge} ERT2cre and *Prdm1*$^{f/+}$B1-8^{ge} ERT2cre naive B cells were mixed at a 1:1 ratio and cotransferred into wild-type CD45.1/1 recipient mice. After immunization with NP-CGG/alum, tamoxifen was administered on day 10, and spleens were analyzed on day 12. Right: Flow cytometry analysis of aCasp3 expression in donor NP$^+$IgG1$^+$CD38$^+$Efnb1$^+$ (Fr.5/6) B cells. Representative of three independent experiments. **, P < 0.01; unpaired Student's t test (B) and *, P < 0.05; paired Student's t test (C). FSC, forward scatter.